Efficient W and Mo deposition and separation with simultaneous hydrogen production in stacked bioelectrochemical systems

Graphical Abstract

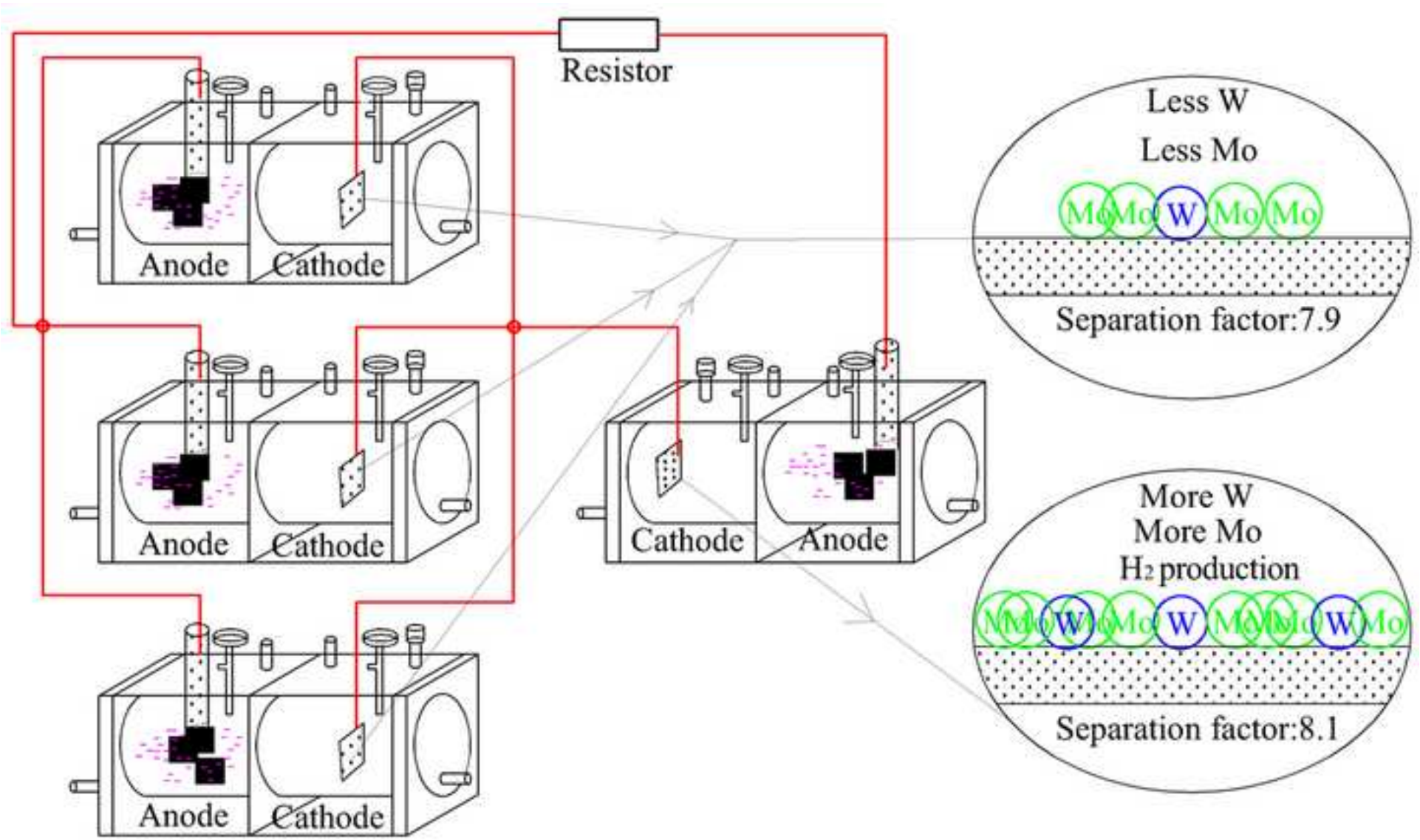

Highlights

→ W and Mo were efficiently deposited in stacked bioelectrochemical systems (BESs);

→ W and Mo were separated from one another in the various units of the stacked BESs;

→ A single BES unit serially matched with three parallel connected units was optimum;

→ The circulation of the catholyte after acidification enhanced W and Mo deposition;

→ Complete separation of W and Mo was achieved after the 7^{th} circulation cycle.

May 28, 2017 R1

Revised manuscript submitted to Chem Eng J

Efficient W and Mo deposition and separation with simultaneous hydrogen production in stacked bioelectrochemical systems

Liping Huang[1,*], Ming Li[1], Yuzhen Pan[2], Yong Shi[1], Xie Quan[1], Gianluca Li Puma[3,*]

1. Key Laboratory of Industrial Ecology and Environmental Engineering, Ministry of Education (MOE), School of Environmental Science and Technology, Dalian University of Technology, Dalian 116024, China

2. College of Chemistry, Dalian University of Technology, Dalian 116024, China

3. Environmental Nanocatalysis & Photoreaction Engineering, Department of Chemical Engineering, Loughborough University, Loughborough LE11 3TU, United Kingdom

Corresponding authors:

(L. Huang) lipinghuang@dlut.edu.cn

(G. Li Puma) g.lipuma@lboro.ac.uk

The authors declare no competing financial interest.

Abstract

Efficient deposition and separation of W(VI) and Mo(VI) with simultaneous hydrogen production, without external energy input, is achieved in stacked bioelectrochemical systems (BESs) composed of microbial fuel cells (MFCs) and microbial electrolysis cells (MECs). The stacked BES-3-1 made of one MEC unit (1#) serially connected with three parallel connected MFC units (2#) outperformed other modules, achieving depositions of 27.6 ± 1.2% (W) and 75.4 ± 2.1% (Mo) with a separation factor of 8.1 ± 0.2 and hydrogen production of 0.34 ± 0.01 m^3/m^3 d in the 1# unit, compared to 12.3 ± 0.9% (W), 52.6 ± 2.2% (Mo) and 7.9 ± 0.5 (separation factor) in the 2# unit. The control experiments with W(VI) only deposited 6.8 ± 1.3% in 1# and 3.3 ± 0.4% in 2#, compared to 65.1 ± 3.2% in 1# and 45.2 ± 0.9% in 2# with Mo(VI) only. The control experiments with either the 1# or 2# unit and a mixture of W(VI) and Mo(VI) deposited 15.3 ± 1.7% (W) and 60.1 ± 1.6% (Mo) (1# only), and 12.9 ± 1.3% (W) and 56.1 ± 2.0% (Mo) (2# only). Reuse of the catholyte after acidification achieved complete separation of W and Mo from one another. This study demonstrates the feasibility of stacked BESs for W and Mo deposition and separation with simultaneous hydrogen production. The dual benefits of W(VI) and Mo(VI) species, and the favorable impact of the 2# unit on the 1# unit in the stacked BES module were critical to achieve efficient performance.

Keywords: bioelectrochemical system; stackable reactor; tungsten and molybdenum deposition; separation factor; hydrogen production

1 Introduction

Tungsten (W) and molybdenum (Mo) are rare transition metals, which impart high-strength, high hardness, good electrical and thermal conductivity, and good corrosion resistance to strong acids to manufactured materials [1]. These metals are extensively used in the manufacturing of advanced materials in key industries, such as the automotive industry. The 2011-12 annual global production was 73000 t for W and 264000 t for Mo, with over 80% of W and nearly 40% of Mo being produced in China [2-3]. The extraction of W and Mo from natural ores involves a significant consumption of energy (11580 kWh/ton) which greatly impacts the environment in terms of air, water and soil pollution [1-4]. Ore dressing wastewater used during the extraction processes contains a significant amount of W and Mo ranging from 10 mg/L to 1000 mg/L [2]. The recovery and separation of these rare metals is therefore desirable from both an environmental and an economical point of view.

Chemical or electrochemical processes conventionally used for the recovery and separation of W(VI) and Mo(VI) involve the use of reducing agents or external electrical energy, which favors the deposition of Mo(VI) while reduced the extraction of W(VI), thus improving the phase separation [1-2,4-8]. However, more efficient and sustainable processes are still needed to achieve efficient W and Mo deposition and for the recovery of each of the two metals.

Bioelectrochemical systems (BESs) may provide an innovative approach for the recovery of metals from wastes and wastewaters [8-12]. Numerous studies have focused on metallurgical BESs for the recovery of individual metals. However, the

practical application of this technology ultimately requires the recovery and simultaneous separation of the multiple metals from the wastewater. Recent studies have investigated the co-deposition of mixed metals on the cathodes of BESs, such as V(V) and Cr(VI) [13], Cu(II), Pb(II), Cd(II), and Zn(II) [14], Zn(II), Pb(II) and Cu(II) [15], Cu(II) and Ni(II) [16], Cu(II) and Cd(II) [17], and Cr(VI), Cu(II) and Cd(II) [18], by an appropriate manipulation of the external applied voltage.

Simultaneously, stacked BESs comprising one microbial fuel cell (MFC) coupled with one microbial electrolysis cell (MEC) have also been conceived for hydrogen production [19], azo dye decolourization [20], recovery of metals of Cr(VI), Cu(II), Cd(II) or tri- and di-valence state cobalt [21-23], and for the separation of mixed metals, including Cu(II), Co(II) and Li(I), and Cr(VI), Cu(II) and Cd(II) [24-27]. The concept of using stacked BESs may provide a sustainable approach to a number of technologies, since stacked BESs are able to be operated without the need of an external energy input (self-powered system). However, currently practical industrial applications may be limited due to the unsatisfactory performance of simply stacked BESs made of two units. In contrast, it is conceivable that multiple BES units appropriately stacked may create a favorable reductive environment on the cathodes, which may yield an efficient recovery and separation of mixed metals from wastewater.

Concerning the recovery and separation of Mo(VI) and W(VI) on the cathodes of BES units, theoretically, Mo(VI) is more spontaneously reduced than W(VI), due to the higher redox potential of the former ((0.53 V against 0.26 V, vs. standard

hydrogen electrode, SHE) using acetate (approximate –0.30 V vs. SHE) as a fuel in the anodic chamber). However, considering the insufficient power output from an individual BES unit, appropriately stacked BESs with varying reducing environments may be conceived, to favor the deposition and separation of W(VI) and Mo(VI) with simultaneous production of hydrogen. This aspect to the authors' knowledge, has not been previously reported.

In contrast to other metals previously explored in stacked BESs, W and Mo own excellent catalytic activities for hydrogen evolution, and can favorably alter the substratum electrode properties, such as surface roughness, conductivity and electrical resistance. Wang et al [28] and Tasić et al. [29] have reported a Ni mesh with W coating and a Au electrode with MoS, both of which exhibited high electrocatalytic activities for hydrogen evolution. In addition, Mo(VI) can act as a catalysis for co-deposition of W(VI) in conventional electrochemical processes [30-31].

In this study, stacked BESs composed of MFCs and MECs in multiple units with serial and/or parallel connection, have been systematically investigated for the deposition and separation of W(VI) and Mo(VI) with simultaneous production of hydrogen. The performance of the stacked BESs was evaluated by linear sweep voltammetry (LSV) and electrochemical impedance spectroscopy (EIS). The reaction products deposited on the electrodes were analyzed by scannning electronic microscopy (SEM), energy dispersive X-ray spectrometry (EDS), X-ray diffraction (XRD) and X-ray photoelectron spectroscopy (XPS). The system parameters including circuital current, W deposition (R_W), Mo deposition (R_{Mo}), separation factor

111 (ε), hydrogen production, cathodic (CE_{ca}) and anodic (CE_{an}) coulombic efficiencies,
112 and overall system efficiency (η_{sys}) were extensively employed to assess system
113 performance. The mutual effect of W(VI) and Mo(VI) species in solution, and the
114 optimization of the stacked BESs have been investigated. This study provides an
115 innovative approach for efficient deposition and separation of W(VI) and Mo(VI)
116 with simultaneous hydrogen production, without the requirement of external energy
117 input.

118 **2 Materials and Methods**

119 *2.1 BES assembly*

120 Identical dual-chamber BESs were used in all experiments, with the chambers
121 separated by a cation exchange membrane (CMI-7000 Membranes International, Glen
122 Rock, NJ). Porous graphite felts (1.0 × 1.0 × 1.0 cm, San ye Co., Beijing, China) were
123 used as anodes, whereas stainless steel sheets (2.0 × 2.0 cm, Qing yuan Co., China)
124 were used as cathodes. The stainless steel sheets were mechanically polished with
125 abrasive papers and cleaned with ethanol and deionized water, before installation [32].
126 The operating volume of the anodic and cathodic chambers of each BES unit was 14
127 mL each.

128 **Here Fig. 1**

129 Nine operational BES configurations comprising a minimum of two and a
130 maximum of six BES units were investigated as shown in Fig. 1, where BES-1-1
131 indicated two units in series, while BES-2-1, BES-3-1 and BES-4-1 represented two,
132 three and four parallel units connected to a single unit in series, respectively. Similarly,
133 the units in parallel were also serially connected with other parallel and single units,

134 respectively. For convenient expression, the reactor units in these modules were
135 denoted in order as 1#, 2# and 3# (Fig. 1). Derived from the concept of MFCs acting
136 as a power source and MECs requiring externally applied voltage (power input)
137 [33-34], the term of applied voltage was specifically used to illustrate that the 2# unit
138 of BES-3-1 acted as a driving force and a power to input voltage to the 1# unit,
139 similar to the previous description [20,22-25]. Data associated with 2# in the BES-3-1
140 have been shown as an average for the units connected in parallel since the differences
141 among the units were insignificant and for the sake of clarity. An external resistor of
142 10 Ω was used to collect the circuital current and the voltage output. A reference
143 electrode (Ag/AgCl, 195 mV vs. SHE) was installed in the cathodic chamber to
144 measure the cathodic potential, with all potentials reported here vs. SHE. All reactors
145 were wrapped with aluminum foil to ensure darkness, to avoid the growth of algae on
146 the anodes and possible side reactions on the cathodes.

147 *2.2 Inoculation and operation*

148 The anodes of the BES were inoculated with suspended bacteria from acetate-fed
149 anodes which were supplemented by an equivalent volume of anolyte solution, to
150 facilitate the acclimation of the anodic biofilms [21-22]. The composition of the
151 anolyte in deionized water was (g/L) sodium acetate 1.0; KH_2PO_4, 4.4; K_2HPO_4, 3.4;
152 NH_4Cl, 1.3; KCl, 0.78; $MgCl_2$, 0.2; $CaCl_2$, 0.0146; NaCl, 0.5; trace vitamins and
153 minerals [35]. The anolyte was sparged with ultrapure N_2 gas for 15 min to remove
154 residual oxygen, prior to transferring to the anodic chambers, whereas deionized water
155 was used as catholyte for anodic exoelectrogens acclimation [24-25]. The acclimation

process was carried out with an external resistor of 1000 Ω which was suitable for bacterial acclimation and avoided inaccurate assessment for subsequent power production [24-25,36-37]. The acclimation period was completed after eight anolyte refreshment cycles, when the anodic potential stabilized at –0.23 ~ –0.27 V vs. SHE, as shown in Fig.S1A. The reactor units were then stacked as shown in Fig. 1. The catholyte was replaced by a solution of Na_2WO_4 and Na_2MoO_4 (1.0 mM each) in deionized water, although the specific concentrations of these two metals in practical wastewaters may vary over a greater range of 0.05 ~ 10.4 mM [1-4]. The initial pH in the catholyte was set to 2.0 and the solution conductivity to 3.5 mS/cm, to reproduce the characteristics of acidic wastewaters containing W(VI) and Mo(VI) [1-3]. The acclimation of the all stacked BES units was completed after two further fed-batch cycle refreshments, which yielded reproducible electrode potentials in all BESs (every operation cycle lasted 4 h). Unless otherwise stated, the stainless steel cathodes were always cleaned in 1.0 M NaOH before each batch cycle operation.

The stability of the cells and the effect of pre-deposited W and Mo on the rate of hydrogen evolution were evaluated using the stacked BES-3-1 configuration, and considering a total of 20 fed-batch operation cycles, avoiding the cleaning of the cathodes. The bare electrodes, and the cathodes of 1# and 2# units in BES-3-1 after the 10^{th} and the 20^{th} operational cycle were analyzed by EIS. The catholyte effluent in the stacked BES-3-1 configuration was totally reused after pH adjustment to 2.5 and at constant solution conductivity (3.5 mS/cm), in order to achieve a higher W and Mo deposition and separation.

Control experiments using catholyte containing either W(VI) or Mo(VI) were performed to evaluate the impact of using a mixture of these two metals on the system performance. Further control experiments under open circuit conditions (OCCs) reflected the effect of circuital current on the metals deposition. Other control experiments using just the 1# unit or just the 2# unit of the BES-3-1 were performed to illustrate the roles that each of these reactor units played on deposition of W and Mo. All stacked reactors were operated in fed-batch mode at room temperature (25 ± 3 °C) and all experiments were conducted in duplicate. The inoculation and solution replacements were performed in an anaerobic glove box (YQX-II, Xinmiao, Shanghai).

2.3 Measurements and analyzes

W(VI) and Mo(VI) in the catholyte and chemical oxygen demand (COD) in the anolyte were measured using standard methods [38]. The pH was measured by a calibrated pH meter (PHS-3C, Leici, Shanghai) and solution conductivity was measured using a conductivity meter (DDS-307, Leici, Shanghai). A glass tube with an inner diameter of 8 mm was glued to the top of the cathodic chambers to create a total headspace of 12 mL [32,39]. Hydrogen in the headspace of the cathodic chambers was sampled using microsyringes (200 μL, Agilent) and analyzed by a gas chromatograph (GC7900, Tianmei, Shanghai) which was equipped with a thermal conductivity detector and a molecular sieve column (TDX-01, 60 – 80, 4 mm × 2 m). The column operating temperature was 110 ºC and the injector and detector temperatures were both 120 ºC. Argon was used as the carrier gas at a constant

pressure of 0.13 MPa [32,39]. Hydrogen production (m^3/m^3 d) was calculated from the hydrogen concentration (m^3/m^3) obtained with the GC, multiplied by the gaseous phase volume (m^3) and divided by the working volume (m^3) and operational time (d).

The morphologies of the electrodes after W and Mo deposition were examined using a scanning electronic microscope (SEM) (QUANTA450, FEI company, USA) equipped with an energy dispersive spectrometer (EDS) (X-MAX 20 mm^2/5- mm^2, Oxford Instruments, UK). X-ray diffraction (XRD-6000, Shimadzu LabX, Japan) and X-ray photoelectron spectroscopy (XPS, Kratos AXIS Ultra DLD) were used to examine the nature and the elemental composition of the crystal products deposited on the cathodes.

The cathode and anode potentials were monitored by an automatic data acquisition system (PISO-813, Hongge Co, Taiwan). Polarization and power density data were obtained with a potentiostat (CHI 760C, Chenhua, Shanghai) using linear sweep voltammetry (LSV). Cyclic voltammetry (CV) (CHI 760C, Chenhua, Shanghai) was carried out with a three-electrode configuration comprising a working electrode (i.e, cathode), a platinum plate counter electrode, and a Ag/AgCl reference electrode. CVs were conducted in solutions with either W(VI) or Mo(VI) species or with a mixture of them, to reflect the reductive peak potentials and reductive peak currents of W(VI) and Mo(VI) under the experimental condition. Both CV and LSV were conducted at a scan rate of 1.0 mV/s. EIS was conducted using the same potentiostat with a three electrode system comprising a working electrode (i.e., cathode), a Ag/AgCl reference electrode (195 mV vs. SHE) located 1 cm away from the cathode

in the cathodic chamber, and a Pt foil (2 × 4 cm) counter electrode placed in the anodic chamber. Impedance analysis was conducted at cathode potentials under OCCs with either the bare electrodes, or the electrodes deposited with W and Mo (obtained after multiple batch cycle operations) in catholyte to determine the impact of the W and Mo deposits on the subsequent W(VI) and Mo(VI) reduction in the stacked BES-3-1. For assessment of effect of W and Mo deposits on subsequent hydrogen evolution, however, impedance analysis was carried out at cathode potentials under CCCs with the same electrodes mentioned above but using catholyte in the absence of W(VI) and Mo(VI). EIS frequency ranged from 100 kHz to 10 mHz, with a sinusoidal perturbation of 10 mV amplitude. The equivalent circuits and detailed values of different resistances were obtained through Zsimpwin software and normalized to the projected area of the cathodes [40-41].

The statistical significance of the experimental data was assessed using a statistical package (SPSS v.19.0) (t-test, $p = 0.05$).

2.4 Calculation

W deposition (R_W, %) and Mo deposition (R_{Mo}, %) were calculated from Eqs. 1 – 2. The power density was normalized to the projected surface area of the separator, allowing the comparison of the results to literature studies based on power per unit area [18,24,42]. The CE_{an}, CE_{ca}, and η_{sys} were calculated from Eqs. 3 – 8 [21] whereas the ε was directly related with R_W and R_{Mo}, and calculated from Eq. 9 [1,8]:

$$R_W = \frac{W(VI)_0 - W(VI)_t}{W(VI)_0} \times 100\% \quad (1)$$

$$R_{Mo} = \frac{Mo(VI)_0 - Mo(VI)_t}{Mo(VI)_0} \times 100\% \quad (2)$$

$$Y_W = \frac{(W(VI)_0 - W(VI)_t) \times V_{ca} \times 32}{(COD_0 - COD_t) \times V_{an}} \quad (3)$$

$$Y_{Mo} = \frac{(Mo(VI)_0 - Mo(VI)_t) \times V_{ca} \times 32}{(COD_0 - COD_t) \times V_{an}} \quad (4)$$

$$Y_{H_2} = \frac{\eta_{H_2} \times V_{H_2} \times 32}{(COD_0 - COD_t) \times V_{an}} \quad (5)$$

$$CE_{an} = \frac{\int_0^t Idt}{96485 \times \frac{4 \times (COD_0 - COD_t) \times V_{an}}{32}} \times 100\% \quad (6)$$

$$CE_{ca} = \frac{[b_1 \times (W(VI)_0 - W(VI)_t) \times V_{ca} + b_2 \times (Mo(VI)_0 - Mo(VI)_t) \times V_{ca} + b_3 \times \eta_{H_2} \times V_{ca}] \times 96485}{\int_0^t Idt} \times 100\% \quad (7)$$

$$\eta_{sys} = \frac{b_1 \times (W(VI)_0 - W(VI)_t) \times V_{ca} + b_2 \times (Mo(VI)_0 - Mo(VI)_t) \times V_{ca} + b_3 \times \eta_{H_2} \times V_{ca}}{(COD_0 - COD_t) \times V_{an} \times \frac{4}{32}} \times 100\% \quad (8)$$

$$\varepsilon = \frac{Mo(VI)_0 - Mo(VI)_t}{Mo(VI)_0} \times \frac{W(VI)_t}{W(VI)_0 - W(VI)_t} = \frac{1 - R_W}{R_W} \times \frac{R_{Mo}}{1 - R_{Mo}} \quad (9)$$

where $W(VI)_0$, $Mo(VI)_0$ and COD_0 are the initial concentrations (mol/L) of W(VI) and Mo(VI) in the catholyte, and of COD in the anolyte of each unit, respectively, and the subscript t refers to the concentration after an operational time of t (h). η_{H2} is the hydrogen concentration (mol/L) at t hours; V_{ca} and V_{an} are the volumes of liquid (L) in the cathodic and anodic chambers, respectively; I is the corresponding circuital current (A); 96485 is the Faraday constant (C/mol e^-); 4 is the molar number of electrons required for oxygen reduction (mol/mol); 32 is the atomic weights of O_2

(g/mol); b_1, b_2 and b_3 are the molar numbers of electrons required for W(VI) and Mo(VI) reduction, and for hydrogen evolution (mol/mol).

3 Results and discussion

3.1 Performance of stacked BES-3-1 configuration

Here Fig. 2

Here Table 1

W and Mo were deposited more efficiently in the stacked BES-3-1 configuration, achieving 27.6 ± 1.2% for W with a yield of 0.09 ± 0.01 mol/mol COD (Fig. 2A and Table 1) and 75.4 ± 2.1% for Mo with 0.26 ± 0.02 mol/mol COD (Fig. 2B and Table 1) in the 1# unit, and 12.3 ± 0.9% with 0.08 ± 0.01 mol/mol COD (W) (Fig. 2A and Table 1) and 52.6 ± 2.2% with 0.23 ± 0.01 mol/mol COD (Mo) (Fig. 2B and Table 1) in the 2# unit. Accordingly, higher CE_{an} of 52 ± 1% in the 1# unit than 42 ± 3% in the 2# unit (p = 0.013), and similar CE_{ca} of 70 ± 5% (1#) and CE_{ca} of 67 ± 1% (2#) (p = 0.15) (Table 1) were observed. These results reflect the higher reductive environment in the 1# unit due to the lower cathode potential (average values in Fig. 2C; as a function of time in Fig. S1B), the higher circuital current (average values in Fig. 2D; as a function of time in Fig. S1B), and the impact of the voltage output from the 2# unit (MFC) which was applied to the 1# unit (MEC) (Fig. 2E).

While the CE_{an} were somewhat lower than values reported for single BES units, particularly those utilizing high efficient Pt-cathodes [33,37], the overall system efficiencies (η_{sys}) were equivalent, and in some cases even higher, to MFC-MEC utilizing graphite granule anodes and cathodes, using $K_3Fe(CN)_6$ and methyl orange as cathodic electron acceptor, respectively [20]. The η_{sys} was slightly lower than in

MFC-MEC with carbon paper anodes and Pt catalyzed cathodes using oxygen and H^+ as cathodic electron acceptor, respectively [19]. The different CE_{an} observed in the 1# and 2# units reflect the existence of different microbial communities, consistent with the corresponding different circuital currents (Fig. 2D). In fact, circuital current is well known to influence microbial community in BESs [33]. Various strategies could be adopted to further increase the CE_{an}, such as through dosing of chemical methane inhibitors (e.g. 2-bromo-ethanesulfonate) [43] or by decreasing the anodic cycle time/hydraulic retention time, to inhibit methane production [44], which subsequently could enhance the amount of cathodic electrons used for the deposition of W and Mo in the stacked BESs.

Under the experimental condition, W(VI) and Mo(VI) reductions occurred at potentials more positive than -0.042 V (Fig. S2), which were more positive than the potentials of the cathodes in the 1# and 2# units (Fig. 2C and S1B), confirming the presence of favorable reductive environments in both units of the stacked BES-3-1. The co-existence of W(VI) and Mo(VI) in solution yielded higher reductive peak currents in comparison to the cases with individual metal salts (Fig. S2), illustrating the dual benefits of W(VI) and Mo(VI) for the occurrence of reduction reactions.

In the control experiments with either the 1# or 2# unit, the amount of W and Mo deposition was 15.3 ± 1.7% (p = 0.000) and 60.1 ± 1.6% (p = 0.000) (1#), and 12.9 ± 1.3% (p = 0.864) (W) and 56.1 ± 2.0% (p = 0.134) (Mo) (2#), respectively (Fig. S3), reflecting that the 2# unit positively affected the performance of 1# unit, whereas the 1# unit negligibly influenced the performance of 2# unit in the stacked BESs. In the

control experiments using catholytes with either W(VI) or Mo(VI), the deposition of W was 6.8 ± 1.3% (1#, p = 0.000) and 3.3 ± 0.4% (2#, p = 0.000) (Fig. 2A) and the deposition of Mo was 65.1 ± 3.2% (1#, p = 0.013) and 45.2 ± 0.9% (2#, p = 0.014) (Fig. 2B), consistent with the results in Fig. S2, reflecting again the dual benefits of W(VI) and Mo(VI) for efficient co-deposition in the stacked BESs. This effect has also been observed in conventional electrochemical processes [30-31]. Note that under OCCs, only 2.9% of W and Mo was deposited, with the single metals and with a mixture of the two metals. A control experiment with only anolyte in the absence of the electrode and exoelectrogens was specifically performed to evaluate the rate of diffusion of W(VI) and/or Mo(VI) from the cathodic to the anodic chambers under OCCs. In parallel, the morphology of the deposits on the cathode electrode was analyzed with SEM-EDS to ascertain the presence of W and/or Mo. The results showed that after a fed batch cycle, the concentrations of W and/or Mo in the anolyte were undetectable, excluding the possibility of W and/or Mo diffusion from the cathode to the anode, although the retention of W and/or Mo on the ion exchange membrane could not be precluded. The detection of W and Mo on the cathode electrode (Fig. S4) confirmed the occurrence of adsorption of W and Mo on the cathode.

Simultaneous with the W(VI) and Mo(VI) co-deposition process, the production of hydrogen in the 1# unit was 0.34 ± 0.01 m^3/m^3 d with a yield of 0.87 ± 0.03 mol/mol COD, compared to the rates obtained with the single metals in the control experiments (0.29 ± 0.00 m^3/m^3 d with Mo(VI) alone (p = 0.193) and 0.15 ± 0.01

m^3/m^3 d with W(VI) alone (p = 0.012)) (Fig. 2F and Table 1). The rate of hydrogen production in the 1# unit of the stacked BES-3-1 was higher than literature results using titanium sheet platinum-coated cathodes in MECs operated at a pH of 6.0 and temperature of 55 ºC (0.2 – 0.3 m^3/m^3 d) [45-46], and was comparable to the rates obtained with the same platinum sheet metal cathodes of MECs at a high applied voltage of 0.9 V but neutral pH (0.68 m^3/m^3 d) [47]. The production of hydrogen in BESs is significantly affected by solution pHs [48]. Taken together with the requirements of H^+ for W(VI) and Mo(VI) reduction as well as hydrogen evolution in the stacked BESs (Eqs. S1-S5), a cathodic pH maintained at 2.0 should favor the highest rate of hydrogen production [48]. As an example, the electron distribution in the stacked BES-3-1 after one batch cycle operation is shown schematically in Fig. S5.

The metal separation factors in the 1# and 2# units were similar (8.1 ± 0.2 and 7.9 ± 0.5, respectively, p = 0.465) (Table 1), which were higher than the value (7.0) reported with a macroporous resin or using manganese dioxide as adsorbent [6,8]. They were also equivalent to the separation factor obtained with $MnSO_4$ as a precipitation reagent [1-2] at the same W(VI) and Mo(VI) concentrations. However, the metal separation factors were lower than those reported with commercial TEVA or macroporous resins (from 14 to 28) at a ratio of W(VI) and Mo(VI) of 1 : 20, and the separation factor of 105, reported using solvent extraction with H_2O_2 as a chelating agent [2,6-7].

Here Fig. 3

The polarization curves with the W(VI) and Mo(VI) mixture (Fig. 3A) were similar to those observed in the control experiments with Mo(VI) alone (Fig. 3C), with maximum power higher than with W(VI) alone (Fig. 3E). These results clearly demonstrate the greater importance of Mo(VI) than W(VI) for delivering maximum power production. Accordingly, the power production in the control experiments with either the 1# or 2# unit (Fig. 3A) reflected more favorably the 2# unit rather than the 1# unit, elucidating that the 2# unit acted as MFCs and that the 1# unit acted as MECs, in the stacked BESs.

The cathodic potentials varied more significantly than the anodic potentials over the current density range (Fig. 3B). Similarly, an increase in current density in the control experiments with either the 1# or 2# unit resulted in more rapid gradients in the cathodic rather than in the anodic potentials (Fig. 3B). These results imply that the performance of the stacked BESs, as well as, each of the 1# and 2# units was augumented by changes in the cathode properties. These results are supported by the increasing consensus that BES performance may be constrained by poor reaction kinetics at the cathode, which results from the complex catholyte composition used and the subsequent multiple competitive reactions that may be generated, the accumulation of OH^- and other products near to the cathode surface and the cathode overpotential [9,49]. The cathode potentials as a function of current density in the controls with Mo(VI) alone (Fig. 3D), decreased more significantly than those obtained with W(VI) alone (Fig. 3F), stressing the greater importance of Mo(VI) rather than W(VI) for determining the cathode potential, consistent with the results in

373 Fig. 2A and B.

374 *3.2 Electrode morphology and product analysis*

375 Products with a smaller area of blue color (Fig. 4A) and with more club-shaped
376 agglomerates (Fig. 4E) were observed in the layer deposited on the cathode of the 1#
377 unit, compared to those observed on the 2# unit (Fig. 4B and F) or on the bare
378 electrode (Fig. S6). The observation of a blue color implies a small amount of reduced
379 Mo and W on the cathodes [1]. The exposure of the deposits to air led to substantial
380 changes in the color (Fig. 4C and D) and microscopic morphology (Fig. 4G and H) in
381 both the 1# (Fig. 4C and G) and 2# units (Fig. 4D and H), implying the sensitivity of
382 the deposits to oxygen. Although the size and shape of the particles deposited on the
383 cathodes were not tightly controlled, the variety of the morphologies observed on
384 these cathodes implies that the different units in the stacked BES-3-1 produced
385 products with different morphologies.

386 EDS analysis of the agglomerates in the deposits of the 1# unit reported higher
387 W (at binding energies of 1.60, 1.78, 8.40 and 9.70 keV) and Mo (at 2.28 keV) signals
388 (Fig. 4I), compared to those observed in the 2# unit (Fig. 4J), confirming the higher
389 efficiency of the 1# unit for metal deposition (Fig. 2A and B). The W content in the
390 products was 2.68% (1#) and 0.67% (2#), well below the 5 – 6% range usually
391 leading to the formation of cracked W and Mo surface [30,50], consistent with the
392 SEM observation in Fig. 4E and F. Exposure to air led to a decrease of the W and Mo
393 signals in both the 1# (Fig. 4K) and 2# units (Fig. 4L), mainly ascribed to the fast
394 oxidation of these reduced products [2,5,30]. The observation of Fe, Cr, Mn, Ni, C

and O on all the cathodes was associated with the composition of the stainless steel substratum. The XRD patterns closely matched $Mo_{8.8}W_{1.2}O_{29}$ (–404) at 24.4° and (302) at 29.7°, and MoO_2 (010) at 63.4° and (102) at 68.7° in the 1# unit (Fig. 4M and Table S1), compared to $Mo_{9.35}W_{1.65}O_{32}$ (–203) at 21.8°, (301) at 25.7° and (–501) at 25.9°, and MoO_2 (404) at 60.9° and (110) at 68.9° in the 2# unit (Fig. 4N and Table S1). Exposure to air completely changed the forms of the crystals in both the 1# (Fig. 4O) and 2# units (Fig. 4P). In concert, the results observed support a significant dependence of the product crystals on the variety of units in the stacked BES-3-1 and that the products were highly sensitive to oxidation.

Here Fig. 5

XPS images displayed the presence of peaks at 35.9 and 38.1 eV for W on all the electrodes (Fig. 5A, C, E and G), which were assigned to W(VI) at W(4f7/2) and W(4f5/2) levels, respectively. However, this could not preclude the oxidation of the highly unstable W(V) as a reduced product during the sample preparation [2,5,30]. In fact, electrodes sampled at the end of one operational cycle, in the absence of N_2 protection, instantly changed in color, implying the weak oxidative character of anionic polymerized W(VI). Accordingly, higher peaks at 234.8 eV and 231.8 eV associated with Mo(V) than those at 231.0 eV and 234.0 eV assigned to Mo(IV) were observed in the 1# unit, both of which were higher than those in the 2# unit (Fig. 5B and Table S2), consistent with the results in Fig. 2B. The reduction of Mo(VI) to Mo(V) was therefore more likely than the reduction towards Mo(IV).

3.3 BESs stacked in different configurations

Here Fig. 6

Among the various configurations of stacked BESs, BES-4-1 comprising a single unit (1#) serially connected with four parallel units (2#) (Fig. 1) exhibited the similar highest deposition of metals to BES-3-1 in the same 1# unit: 28.7 ± 0.7% (W) (p = 0.528) (Fig. 6A) and 69.1 ± 1.3% (Mo) (p = 0.15) (Fig. 6B). In the 2# unit, however, Mo deposition of 39.3 ± 1.7% in BES-4-1 (Fig. 6B) was lower than 52.6 ± 2.2% in BES-3-1 (p = 0.042) (Fig. 2B), compared to the similar W deposition (13.2 ± 1.6% in BES-4-1, 12.3 ± 0.9% in BES-3-1, p = 0.684). As a consequence, separation factor of 4.3 ± 0.1 in the 2# unit of BES-4-1 was significantly lower than 7.9 ± 0.5 in BES-3-1 based on Eq. 9 (Table 1). While hydrogen production of 0.83 ± 0.20 m^3/m^3 d in BES-4-1 was higher than 0.34 ± 0.10 m^3/m^3 d in BES-3-1 (Table 1), the yield of hydrogen in BES-4-1 (0.56 ± 0.01 mol/mol COD) was lower than in BES-3-1 (0.87 ± 0.03 mol/mol COD), explained by the higher rate of COD consumption in the BES-4-1 anode, according to Eq. 5. Taken together, BES-4-1 had an advantage of more hydrogen production over BES-3-1 whereas the latter favored for more Mo deposition and the subsequent more efficient W and Mo separation. Considering the merit of favor for more metal deposition and separation in BES-3-1, this stacked BES-3-1 module was thus selected to evaluate the effect of multiple cycles operation, and the effect of effluent reuse from the 1# and 2# units, for complete separation of W from Mo.

It should be noted that each of these reactor units could independently generate current prior connection in stacked BESs. BES-2-1, BES-3-1 and BES-4-1 modules were made of MECs (1#) and MFCs (2#, associated two, three or four units in a

parallel connection). These stacked systems operated spontaneously at voltage outputs higher than that from coupled single units (1#), since the internal resistance, in the parallel connected units, progressively decreased as the number of parallel connected units increased. Therefore, at a fixed external resistance (e.g. 1#), the stacked BESs would spontaneously evolve hydrogen, as long as the voltage output from the units connected in parallel (e.g. 2#) could produce a more negative cathodic potentials in the 1# unit, sufficient for H^+ reduction (theoretically –0.135 V at the present initial pH of 2.0) [34]. The hydrogen production rate, however, dynamically depended on the circuital current of the BESs [34]. Thus, hydrogen was thermodynamically evolved in the 1# unit rather than the 2# unit, evolving a higher hydrogen production rate in BES-4-1 rather than in BES-3-1 (Fig. 2C and 6C, Table 1). However, the inadequate cathodic potential and circuital currents in the 1# unit of BES-2-1 resulted in negligible evolution of hydrogen (Table 1 and Fig. 6C and 6D). In BES-3-2-1, the three units connected in parallel acted as MFCs, while the two units in parallel serially stacked with a single unit, served as MECs. The hydrogen production in BES-3-2-1 was reasonably lower than the 1# unit of BES-3-1 due to the more number of units being driven in the former (Table 1). The BESs with equal number of serial and/or parallel connected units including BES-1-1, BES-2-2, BES-3-3, BES-1-1-1 and BES-2-2-2, produced similar voltage outputs and net electricity was always produced, excluding the possibility of hydrogen evolution in these systems.

3.4 BES long-term stability

Here Fig. 7

The deposition of W in both the 1# and 2# units of the BES-3-1 exhibited a

463 decreasing trend with operational time, from 27.6 ± 1.2 % (1#) and 12.3 ± 0.9 % (2#)
464 in the first cycle to 10.1 ± 1.3% (1#) and 8.4 ± 0.8% (2#) after the 20th cycle (Fig. 7A).
465 Conversely, Mo deposition in the 2# unit gradually increased, from the initial 52.6 ±
466 2.2% (1st cycle) to 61.6 ± 2.2% (20th cycle) (Fig. 7B). The insignificant change in the
467 deposition of Mo in the 1# unit (71.7 – 75.4%) was accompanied with an increase in
468 hydrogen production (Table S3), reflecting the beneficial catalytic effect of the Mo
469 deposit on hydrogen evolution [29]. Specifically, it has been shown that MoS_2
470 particles coated carbon cloth performs better than bare stainless steel and even
471 surpasses platinum-based electrodes for hydrogen evolution [51].

472 The separation factor in BES-3-1 increased from 8.1 ± 1.4 (1#) and 7.9 ± 0.0 (2#)
473 (1st cycle) to 22.8 ± 1.9 (1#) and 17.7 ± 0.8 (2#) (20th cycle) (Fig. 7C), suggesting a
474 beneficial effect of the operational time on the separation of the metals.

475 Cathode potentials (Fig. 7D), circuital current (Fig. 7E), applied voltage (Fig.
476 7F) and hydrogen production (Table S3) increased progressively up to a maximum at
477 the 10th cycle, which were consistent with the polarization curves (Fig. S8) and with
478 the appreciable deposition of W and Mo on the electrodes (Fig. 7A and B). Such
479 results are further supported by the positive effect of tungsten and molybdenum oxide
480 impregnated electrodes in MFCs for power production and V(V) or O_2 reduction
481 [52-54]. Further deposition of the metals from the 11th to 20th cycle, resulted in a
482 decrease in the circuital current (Fig. 7E) and negligible changes in the cathode
483 potential (Fig. 7D), which ultimately led to a decrease of the hydrogen production
484 with operational time (Table S3). This last effect could be attributed to an excessive

accumulation of metals on the electrodes, which was further proved as follows.

The EIS spectra were fitted to equivalent circuits (Fig. S9) to identify the components determining the internal resistances in the BES-3-1 after the 10^{th} and 20^{th} cycle, for assessing W(VI) and Mo(VI) reduction, and hydrogen evolution (Fig. S10 and Table S4) in comparison with the bare electrodes. The diffusional resistance (R_d) for W(VI) and Mo(VI) reduction was significantly higher than the polarization (R_p) and the ohmic (R_o) resistances (Fig. S10A and Table S4) due to the mass transfer limitation of the formed macromolecules of W and Mo heteropolyacid [1-2]. Compared to the bare electrode, the R_d, R_p and R_o resistances after the 10^{th} cycle substantially decreased to 4252.3 Ω, 43.2 Ω and 14.8 Ω (1#) and 2076.7 Ω, 25.4 Ω and 14.2 Ω (2#), respectively, which were consistent with the enhanced system performance due to the presence of W and Mo deposits (Fig. 7). However, at the 20^{th} cycle, R_d and R_p increased, while R_o negligibly changed, which was attributed to the excessive W and Mo layer formed.

With respect to the bare electrode having R_p of 89.4 Ω, R_d of 4897.2 Ω and R_o of 18.2 Ω for hydrogen evolution (Fig. S10B and Table S4), the rate of hydrogen production increased after a prolonged operation (10^{th} cycle) (Table S3) due to the decrease of the resistance, R_p (22.7 Ω), R_d (503.5 Ω) and R_o (7.3 Ω). However, further use (20^{th} cycle) led to an increase in the resistances, R_p (43.4 Ω), R_d (1123.4 Ω) and R_o (10.5 Ω) (Table S4) and, in consequence, to a decrease in the rate of hydrogen production (Table S3), consistent with the EIS results for W(VI) and Mo(VI) reduction (Fig. S10A and Table S4). These results, in concert, clearly demonstrated

that the decreased rate of hydrogen production at the 20th cycle resulted from the excessive layer of W and Mo built on the cathodes of 1# in the stacked BESs.

3.5 Catholyte effluent reuse

The catholyte effluent after acidic adjustment was fully reused in the BES-3-1 to increase the amount of metal deposited, which reached 36.0 ± 0.3% (W) and 99.4 ± 0.5% (Mo) in the 1# unit, and 26.9 ± 0.2% (W) and 96.2 ± 0.6% (Mo) in the 2# unit at the 7th circulation (Fig. S11A and B). Accordingly, a significantly higher separation factor equal to 467 ± 22 was reached in the 1# unit, compared to 70 ± 3 in the 2# unit (Fig. S11C). This separation factor achieved in the 1# unit was higher than that observed with ion exchange resins, solvent extraction, or MnO_2 and $MnSO_4$ adsorbents (range 7 – 105) [2,6-8]. A decrease of the concentration of W(VI) and Mo(VI) in the catholyte with reuse led to a decrease of the circuital current (Fig. S11D), the cathode potential (Fig. S11E), and the applied voltage to the 1# unit (Fig. S11F) as expected, due to the progressive reduction of W(VI) and Mo(VI) electron acceptors in the catholyte. This result was consistent with the reports using other multiple metals as electron acceptors in BESs [17-18,55-56]. The pH of the catholyte after each reuse always increased in both the 1# (Fig. S11G) and the 2# unit (Fig. S11H), and required a pre-acidification step to promote efficient W and Mo deposition and separation.

On the basis of the operating costs alone, the net value of W and Mo products recovered from the system (7.22 $ per m^3 mixed W(VI) and Mo(VI)) was significantly higher than the cost required for acidification of the catholyte (0.03 $/$m^3$),

demonstrating the economical feasibility of this technology.

With regard to the practical application of stacked BESs for W and Mo recovery, the two-chamber BESs have merits over the one-chamber systems, since these avoid the toxicity of W and Mo to the anodic exoelectrogens while permitting the simultaneous treatment of two different wastewaters [9-10]. Considering that the materials costs are steadily decreasing, particularly the costs of the ion exchange membrane [27,42,55,57], cost-effective two-chamber stacked BESs are promising systems for sustainable recovery and separation of W and Mo at industrial scale, with simultaneous production of hydrogen. However, the practical implementation of this technology for industrial wastewater treatment requires further pilot and full-scale investigations, to evaluate the long-term operation and stability of the system over feeds with fluctuating characteristics [57]. In addition, in this study we have adjusted the pH to the acidic value of 2.0 only at the beginning of the experiment, although a recent study suggests that a pH control during the entire operational period to acidic values may lead to enhanced performance [48]. This aspect should be investigated in further studies. The separation of the W and Mo layer deposited on the electrodes may also represent a further challenge for the practical application of this technology. However, the in-situ utilization of these deposits for photocatalytic processes may become an attractive strategy for reuse, since W and Mo oxides exhibits excellent photocatalytic properties [58]. It is expected that further optimization of pH control, and ratio of W(VI) and Mo(VI) would result in an improved performance of the stacked BESs presented in this study.

4 Conclusions

This study demonstrated a novel method for the deposition and separation of W and Mo metals in stacked BESs with simultaneous hydrogen production, without the need of external energy input. The optimized stacked module was the BES-3-1, where the dual benefits of the W(VI) and Mo(VI) species, and the favorable impact of the 2# unit on the 1# unit were observed, with simultaneous hydrogen production. This system also displayed a favorable configuration in which the 2# MFC unit assisted the 1# MEC unit. Further reuse of the catholyte after acidification led to complete separation of W and Mo from one another. Since W(VI) and Mo(VI) are extensively present in ore dressing wastewater, this study may provide a sustainable and environmentally benign approach to this industry for efficient recovery and separation of W and Mo with simultaneous hydrogen production.

Acknowledgments

The authors gratefully acknowledge financial support from the National Natural Science Foundation of China (No. 51578104), and the Programme of Introducing Talents of Discipline to University (B13012).

References

[1] Z. Zhao, C. Cao, X. Chen, G. Huo, Separation of macro amounts of tungsten and molybdenum by selective precipitation, Hydrometallurgy 108 (2011) 229-232.

[2] T.A. Lasheen, M.E. El-Ahmady, H.B. Hassib, A.S. Helal, Molybdenum metallurgy review: hydrometallurgical routes to recovery of molybdenum from ores and mineral raw materials, Mineral Processing Extractive Metall. Rev. 36 (2015) 145-173.

[3] T. Ogi, T. Makino, K. Okuyama, W.J. Stark, F. Iskandar, Selective biosorption and

recovery of tungsten from an urban mine and feasibility evaluation, Ind. Eng. Chem. Res. 55 (2016) 2903-2910.
[4] P. Nekovář, Schrötterová, Extraction of V(V), Mo(VI) and W(VI) polynuclear species by primene JMT, Chem. Eng. J. 79 (2000) 229-233.
[5] B.P. Hahn, K.J. Stevenson, Cathodic electrodeposition of mixed molybdenum-selenium oxides, J. Electroanal. Chem. 638 (2010) 151-160.
[6] W.J. Guan, G.Q. Zhang, L.S. Xiao, D.Z. Wang, Continuous running test of the solvent extraction separation of Mo and W by H_2O_2-complexation with TRPO/TBP, Hydrometallurgy 157 (2015) 1-8.
[7] W. Zhang, J. Li, Z. Zhao, S. Huang, X. Chen, K. Hu, Recovery and separation of W and Mo from high-molybdenum synthetic scheelite in HCl solutions containing H_2O_2, Hydrometallurgy 155 (2015) 1-5.
[8] Y. Song, X. Chen, Z. Zhao, J. Zhang, L. He, Theoretical basis for the separation of W and Mo with manganese dioxide: a speciation-based approach, Metall. Mater. Trans. B. 47B (2016) 675-685.
[9] H. Wang, Z.J. Ren, Bioelectrochemical metal recovery from wastewater: a review, Water Res. 66 (2014) 219-232.
[10] Y.V. Nancharaiah, S.V. Mohan, P.N.L. Lens, Biological and bioelectrochemical recovery of critical and scarce metals, Trend Biotechnol. 34 (2016) 137-155.
[11] S.M. Iskander, B. Brazil, J.T. Novak, Z. He, Resource recovery from landfill leachate using bioelectrochemical systems: Opportunities, challenges, and perspectives, Bioresour. Technol. 201 (2016) 347-354.
[12] L. Huang, R. Guo, L. Jiang, X. Quan, G. Chen, Cobalt leaching from lithium cobalt oxide in microbial electrolysis cells, Chem. Eng. J. 220 (2013) 72-80.
[13] B. Zhang, C. Feng, J. Ni, J. Zhang, W. Huang, Simultaneous reduction of vanadium (V) and chromium (VI) with enhanced energy recovery based on microbial fuel cell technology, J. Power Sources 204 (2012) 34-39.
[14] O. Modin, X. Wang, X. Wu, S. Rauch, K.K. Fedje, Bioelectrochemical recovery of Cu, Pb, Cd, and Zn from dilute solutions, J. Hazard. Mater. 235-236 (2012) 291-297.
[15] H. Tao, T. Lei, G. Shi, X. Sun, X. Wei, L. Zhang, W. Wu, Removal of heavy metals from fly ash leachate using combined bioelectrochemical systems and electrolysis, J. Hazard. Mater. 264 (2014) 1-7.
[16] H. Luo, G. Liu, R. Zhang, Y. Bai, S. Fu, Y. Hou, Heavy metal recovery combined with H-2 production from artificial acid mine drainage using the microbial electrolysis cell, J. Hazard. Mater. 270 (2014) 153-159.
[17] Q. Wang, L. Huang, Y. Pan, P. Zhou, X. Quan, B.E. Logan, H. Chen, Cooperative cathode electrode and in situ deposited copper for subsequent enhanced Cd(II) removal and hydrogen evolution in bioelectrochemical systems, Bioresour. Technol. 200 (2016) 565-571.
[18] L. Huang, Q. Wang, L. Jiang, P. Zhou, X. Quan, B.E. Logan, Adaptively evolving bacterial communities for complete and selective reduction of Cr(VI), Cu(II) and Cd(II) in biocathode bioelectrochemical systems, Environ. Sci. Technol. 49 (2015) 9914-9924.

621 [19] M. Sun, G. Sheng, L. Zhang, C. Xia, Z. Mu, X. Liu, H. Wang, H. Yu, R. Qi, T. Yu,
622 M. Yang, An MEC-MR-coupled system for biohydrogen production from acetate,
623 Environ. Sci. Technol. 42 (2008) 8095-8100.
624 [20] Y. Li, H. Yang, J. Shen, Y. Mu, H. Yu, Enhancement of azo dye decolourization in
625 a MFC-MEC coupled system, Bioresour. Technol. 202 (2016) 93-100.
626 [21] L. Huang, B. Yao, D. Wu, X. Quan, Complete cobalt recovery from lithium
627 cobalt oxide in self-driven microbial fuel cell - microbial electrolysis cell systems, J.
628 Power Sources 259 (2014) 54-64.
629 [22] Y. Zhang, L. Yu, D. Wu, L. Huang, P. Zhou, X. Quan, G. Chen, Dependency of
630 simultaneous Cr(VI), Cu(II) and Cd(II) reduction on the cathodes of microbial
631 electrolysis cells self-driven by microbial fuel cells, J. Power Sources 273 (2015)
632 1103-1113.
633 [23] J. Shen, Y. Sun, L. Huang, J. Yang, Microbial electrolysis cells with biocathodes
634 and driven by microbial fuel cells for simultaneous enhanced Co(II) and Cu(II)
635 removal, Front. Environ. Sci. Eng. 9 (2015) 1084-1095.
636 [24] D. Wu, Y. Pan, L. Huang, X. Quan, J. Yang, Comparison of Co(II) reduction on
637 three different cathodes of microbial electrolysis cells driven by Cu(II)-reduced
638 microbial fuel cells under various cathode volume conditions, Chem. Eng. J. 266
639 (2015) 121-132.
640 [25] D. Wu, Y. Pan, L. Huang, P. Zhou, X. Quan, H. Chen, Complete separation of
641 Cu(II), Co(II) and Li(I) using self-driven MFCs-MECs with stainless steel mesh
642 cathodes under continuous flow conditions, Sep. Purif. Technol. 147 (2015)
643 114-124.
644 [26] M. Li, Y. Pan, L. Huang, Y. Zhang, J. Yang, Continuous flow operation with
645 appropriately adjusting composites in influent for recovery of Cr(VI), Cu(II) and
646 Cd(II) in self-driven MFC-MEC system, Environ. Technol. 38 (2017) 615-628.
647 [27] X. Chen, P. Liang, X. Zhang, X. Huang, Bioelectrochemical systems-driven
648 directional ion transport enables low-energy water desalination, pollutant removal,
649 and resource recovery, Bioresour. Technol. 215 (2016) 274-284.
650 [28] T. Wang, L. Liu, Z. Zhu, P. Papakonstantinou, J. Hu, H. Liu, M. Li, Enhanced
651 electrocatalytic activity for hydrogen evolution reaction from self-assembled
652 monodispersed molybdenum sulfide nanoparticles on an Au electrode, Energy
653 Environ. Sci. 6 (2013) 625-633.
654 [29] G.S. Tasić, U. Lačnjevac, M.M. Tasić, M.M. Kaninski, V.M. Nikolić, D.L. Žugić,
655 V.D. Jović, Influence of electrodeposition parameters of Ni-W on Ni cathode for
656 alkaline water electrolyser, Inter. J. Hydrogen Energy 38 (2013) 4291-4297.
657 [30] S. Sun, T. Bairachna, E.J. Podlaha, Induced codeposition behavior of
658 electrodeposited NiMoW alloys, J. Electrochem. Soc. 160 (2013) D434-D440.
659 [31] F. Jiang, Y. Zhang, N. Sun, J. Leng, Tungsten coating prepared on molybdenum
660 substrate by electrodeposition from molten salt in air atmosphere, Appl. Surf. Sci.
661 327 (2015) 432-436.
662 [32] Q. Wang, L. Huang, H. Yu, X. Quan, Y. Li, G. Fan, L. Li, Assessment of five
663 different cathode materials for Co(II) reduction with simultaneous hydrogen
664 evolution in microbial electrolysis cells, Inter. J. Hydrogen Energy 40 (2015)

184-196.
[33] B.E. Logan, Essential data and techniques for conducting microbial fuel cell and other types of bioelectrochemical system experiments, ChemSusChem 5 (2012) 988-994.
[34] A. Kadier, M.S. Kalil, P. Abdeshahian, K. Chandrasekhar, A. Mohamed, N.F. Azman, W. Logroño, Y. Simayi, A.A. Hamid, Recent advances and emerging challenges in microbial electrolysis cells (MECs) for microbial production of hydrogen and value-added chemicals. Renew Sust Energ Rev 61 (2016) 501-525.
[35] L. Huang, L. Gan, N. Wang, X. Quan, B.E. Logan, G. Chen, Mineralization of pentachlorophenol with enhanced degradation and power generation from air cathode microbial fuel cells, Biotechnol. Bioeng. 109 (2012) 2211-2221.
[36] Z.Y. Ren, H.J. Yan, W. Wang, M.M. Mench, J.M. Regan, Characterization of microbial fuel cells at microbially and electrochemically meaningful time scales, Environ. Sci. Technol. 45 (2011) 2435-2441.
[37] W. Yang, K.Y. Kim, P.E. Saikaly, B.E. Logan, The impact of new cathode materials relative to baseline performance of microbial fuel cells all with the same architecture and solution chemistry, Energy Environ. Sci. DOI: 10.1039/C7EE00910K.
[38] State Environment Protection Administration, the Water and Wastewater Monitoring Methods, fourth ed., China Environmental Science Press, Beijing, 2002.
[39] Y. Chen, J. Shen, L. Huang, Y. Pan, X. Quan, Enhanced Cd(II) removal with simultaneous hydrogen production in biocathode microbial electrolysis cells in the presence of acetate or $NaHCO_3$, Inter. J. Hydrogen Energy 41 (2016) 13368-13379.
[40] Z. He, F. Mansfeld, Exploring the use of electrochemical impedance spectroscopy (EIS) in microbial fuel cell studies, Energy Environ. Sci. 2 (2009) 215-219.
[41] D. Wu, L. Huang, X. Quan, G. Li Puma, Electricity generation and bivalent copper reduction as a function of operation time and cathode electrode material in microbial fuel cells, J. Power Sources 307 (2016) 705-714.
[42] W. Li, G. Sheng, X. Liu, H. Yu, Recent advances in the separators for microbial fuel cells, Bioresour. Technol. 102 (2011) 244-252.
[43] K.J. Chae, M.J. Choi, K.Y. Kim, F.F. Ajayi, W. Park, C.W. Kim, I.S. Kim, Methanogenesis control by employing various environmental stress conditions in two-chambered microbial fuel cells, Bioresour. Technol. 101 (2010) 5350-5357.
[44] T.H.J.A. Sleutels, R. Lodder, H.V.M. Hamelers, C.J.N. Buisman, Improved performance of porous bio-anodes in microbial electrolysis cells by enhancing mass and charge transport, Inter. J. Hydrogen Energy 34 (2009) 9655-9661.
[45] R.A. Rozendal, H.V.M. Hamelers, G.J.W. Euverink, S.J. Metz, C.J.N. Buisman, Principle and perspectives of hydrogen production through biocatalyzed electrolysis, Inter. J. Hydrogen Energy 31 (2006) 1632-1640.
[46] M.C. Dictor, C. Joulian, S. Touzé, I. Ignatiadis, D. Guyonnet, Electro-stimulated biological production of hydrogen from municipal solid waste, Inter. J. Hydrogen Energy 35 (2010) 10682-10692.

[47] P.A. Selembo, M.D. Merrill, B.E. Logan, The use of stainless steel and nickel alloys as low-cost cathodes in microbial electrolysis cells, J. Power Sources 190 (2009) 271-278.
[48] Y. Ruiz, J.A. Baeza, A. Guisasola, Enhanced performance of bioelectrochemical hydrogen production using a pH control strategy, ChemSusChem 8 (2015) 389-397.
[49] X. Liu, W. Li, H. Yu, Cathodic catalysts in bioelectrochemical systems for energy recovery from wastewater, Chem. Soc. Rev. 43 (2014) 7718-7745.
[50] H. Cesiulis, A. Baltutiene, M. Donten, M.L. Donten, Z. Stojek, Increase in rate of electrodeposition and in Ni(II) concentration in the bath as a way to control grain size of amorphous/nanocrystalline Ni-W alloys, J. Solid State Electrochem. 6 (2002) 237-244.
[51] J.C. Tokash, B.E. Logan, Electrochemical evaluation of molybdenum disulfide as a catalyst for hydrogen evolution in microbial electrolysis cells, Inter. J. Hydrogen Energy 36 (2011) 9439-9445.
[52] Y. Shen, H. Xu, P. Xu, X. Wu, Y. Dong, L. Lu, Electrochemical catalytic activity of tungsten trioxide-modified graphite felt toward VO_2^+/VO^{2+} redox reaction, Electrochim. Acta 132 (2014) 37-41.
[53] E. Yavuz, K.V. Özdokur, İ. Çakar, S. Koçak, F.N. Ertaş, Electrochemical preparation, characterization of molybdenum-oxide/platinum binary catalysts and its application to oxygen reduction reaction in weakly acidic medium, Electrochim. Acta 151 (2015) 72-80.
[54] J.L. Varanasi, A.K. Nayak, Y. Sohn, D. Pradhan, D. Das, Improvement of power generation of microbial fuel cell by integrating tungsten oxide electrocatalyst with pure or mixed culture biocatalysts, Electrochim. Acta 199 (2016) 154-163.
[55] C. He, Z. Mu, H. Yang, Y. Wang, Y. Mu, H. Yu, Electron acceptors for energy generation in microbial fuel cells fed with wastewaters: A mini-review, Chemosphere 140 (2015) 12-17.
[56] Q. Wang, L. Huang, Y. Pan, X. Quan, G. Li Puma, Impact of Fe(III) as an effective electron-shuttle mediator for enhanced Cr(VI) reduction in microbial fuel cells: Reduction of diffusional resistances and cathode overpotentials, J. Hazard. Mater. 321 (2016) 896-906.
[57] W. Li, H. Yu, Z. He, Towards sustainable wastewater treatment by using microbial fuel cells-centered technologies, Energy Environ. Sci. 7 (2014) 911-924.
[58] R.O. Ramabhadran, J.E. Mann, S.E. Waller, D.W. Rothgeb, C.C. Jarrold, K. Raghavachari, New insights on photocatalytic H_2 liberation from water using transition-metal oxides: Lessons from cluster models of molybdenum and tungsten oxides, J. Am. Chem. Soc. 135 (2013) 17039-17051.

Table 1 Separation factor, product yield, and operational efficiencies in various stacked BESs.

Fig. 1 Types of stacked BESs in this study

Fig. 2 W (A) and Mo (B) deposition, cathode potentials (C) and circuital current (D)

in the stacked BES-3-1. Applied voltage (E) and hydrogen production (F) in the 1# unit of the BES-3-1.

Fig. 3 Voltage output and power density (A, C and E), and anode and cathode potentials (B, D and F) in the stacked BES-3-1, and controls of the single 1# or 2# units with the components of W(VI) and Mo(VI) (A and B), individual Mo(VI) (C and D), and single W(VI) (E and F).

Fig. 4 Naked eye (A, B, C and D) and SEM (E, F, G and H) observation, EDS analysis (I, J, K and L) and XED determination (M, N, O and P) on the cathodes of the 1# (A, E, I, M, C, G, K and O) and 2# units (B, F, J, N, D, H, L and P) before (A, E, I, M, B, F, J and N) and after (C, G, K, O, D, H, L and P) exposed to air for 24 h (2 cycle operation).

Fig. 5 XPS analysis for W (A, C, E and G) and Mo (B, D, F and H) elements on the cathodes of the 1# (A, B, E, and F) and 2# units (C, D, G and H) before (A, B, C and D) and after (E, F, G and H) exposed to air for 24 h.

Fig. 6 W (A) and (B) Mo deposition in the different units of the stacked BESs and the associated cathode potential (C) and circuital current (D).

Fig. 7 W (A) and Mo (B) deposition, separation factor (C), cathode potential (D), and circuital current (E) in the 1# and 2# units of BES-3-1, as well as applied voltage as a function of the operational cycle.

May 28, 2017 R1

Revised manuscript submitted to Chem Eng J

Efficient W and Mo deposition and separation with simultaneous hydrogen production in stacked bioelectrochemical systems

Liping Huang[1,*], Ming Li[1], Yuzhen Pan[2], Yong Shi[1], Xie Quan[1], Gianluca Li Puma[3,*]

1. Key Laboratory of Industrial Ecology and Environmental Engineering, Ministry of Education (MOE), School of Environmental Science and Technology, Dalian University of Technology, Dalian 116024, China

2. College of Chemistry, Dalian University of Technology, Dalian 116024, China

3. Environmental Nanocatalysis & Photoreaction Engineering, Department of Chemical Engineering, Loughborough University, Loughborough LE11 3TU, United Kingdom

Corresponding authors:

(L. Huang) lipinghuang@dlut.edu.cn

(G. Li Puma) g.lipuma@lboro.ac.uk

The authors declare no competing financial interest.

Abstract

Efficient deposition and separation of W(VI) and Mo(VI) with simultaneous hydrogen production, without external energy input, is achieved in stacked bioelectrochemical systems (BESs) composed of microbial fuel cells (MFCs) and microbial electrolysis cells (MECs). The stacked BES-3-1 made of one MEC unit (1#) serially connected with three parallel connected MFC units (2#) outperformed other modules, achieving depositions of 27.6 ± 1.2% (W) and 75.4 ± 2.1% (Mo) with a separation factor of 8.1 ± 0.2 and hydrogen production of 0.34 ± 0.01 m^3/m^3 d in the 1# unit, compared to 12.3 ± 0.9% (W), 52.6 ± 2.2% (Mo) and 7.9 ± 0.5 (separation factor) in the 2# unit. The control experiments with W(VI) only deposited 6.8 ± 1.3% in 1# and 3.3 ± 0.4% in 2#, compared to 65.1 ± 3.2% in 1# and 45.2 ± 0.9% in 2# with Mo(VI) only. The control experiments with either the 1# or 2# unit and a mixture of W(VI) and Mo(VI) deposited 15.3 ± 1.7% (W) and 60.1 ± 1.6% (Mo) (1# only), and 12.9 ± 1.3% (W) and 56.1 ± 2.0% (Mo) (2# only). Reuse of the catholyte after acidification achieved complete separation of W and Mo from one another. This study demonstrates the feasibility of stacked BESs for W and Mo deposition and separation with simultaneous hydrogen production. The dual benefits of W(VI) and Mo(VI) species, and the favorable impact of the 2# unit on the 1# unit in the stacked BES module were critical to achieve efficient performance.

Keywords: bioelectrochemical system; stackable reactor; tungsten and molybdenum deposition; separation factor; hydrogen production

1 Introduction

Tungsten (W) and molybdenum (Mo) are rare transition metals, which impart high-strength, high hardness, good electrical and thermal conductivity, and good corrosion resistance to strong acids to manufactured materials [1]. These metals are extensively used in the manufacturing of advanced materials in key industries, such as the automotive industry. The 2011-12 annual global production was 73000 t for W and 264000 t for Mo, with over 80% of W and nearly 40% of Mo being produced in China [2-3]. The extraction of W and Mo from natural ores involves a significant consumption of energy (11580 kWh/ton) which greatly impacts the environment in terms of air, water and soil pollution [1-4]. Ore dressing wastewater used during the extraction processes contains a significant amount of W and Mo ranging from 10 mg/L to 1000 mg/L [2]. The recovery and separation of these rare metals is therefore desirable from both an environmental and an economical point of view.

Chemical or electrochemical processes conventionally used for the recovery and separation of W(VI) and Mo(VI) involve the use of reducing agents or external electrical energy, which favors the deposition of Mo(VI) while reduced the extraction of W(VI), thus improving the phase separation [1-2,4-8]. However, more efficient and sustainable processes are still needed to achieve efficient W and Mo deposition and for the recovery of each of the two metals.

Bioelectrochemical systems (BESs) may provide an innovative approach for the recovery of metals from wastes and wastewaters [8-12]. Numerous studies have focused on metallurgical BESs for the recovery of individual metals. However, the

practical application of this technology ultimately requires the recovery and simultaneous separation of the multiple metals from the wastewater. Recent studies have investigated the co-deposition of mixed metals on the cathodes of BESs, such as V(V) and Cr(VI) [13], Cu(II), Pb(II), Cd(II), and Zn(II) [14], Zn(II), Pb(II) and Cu(II) [15], Cu(II) and Ni(II) [16], Cu(II) and Cd(II) [17], and Cr(VI), Cu(II) and Cd(II) [18], by an appropriate manipulation of the external applied voltage.

Simultaneously, stacked BESs comprising one microbial fuel cell (MFC) coupled with one microbial electrolysis cell (MEC) have also been conceived for hydrogen production [19], azo dye decolourization [20], recovery of metals of Cr(VI), Cu(II), Cd(II) or tri- and di-valence state cobalt [21-23], and for the separation of mixed metals, including Cu(II), Co(II) and Li(I), and Cr(VI), Cu(II) and Cd(II) [24-27]. The concept of using stacked BESs may provide a sustainable approach to a number of technologies, since stacked BESs are able to be operated without the need of an external energy input (self-powered system). However, currently practical industrial applications may be limited due to the unsatisfactory performance of simply stacked BESs made of two units. In contrast, it is conceivable that multiple BES units appropriately stacked may create a favorable reductive environment on the cathodes, which may yield an efficient recovery and separation of mixed metals from wastewater.

Concerning the recovery and separation of Mo(VI) and W(VI) on the cathodes of BES units, theoretically, Mo(VI) is more spontaneously reduced than W(VI), due to the higher redox potential of the former ((0.53 V against 0.26 V, vs. standard

89 hydrogen electrode, SHE) using acetate (approximate –0.30 V vs. SHE) as a fuel in
90 the anodic chamber). However, considering the insufficient power output from an
91 individual BES unit, appropriately stacked BESs with varying reducing environments
92 may be conceived, to favor the deposition and separation of W(VI) and Mo(VI) with
93 simultaneous production of hydrogen. This aspect to the authors' knowledge, has not
94 been previously reported.

95 In contrast to other metals previously explored in stacked BESs, W and Mo own
96 excellent catalytic activities for hydrogen evolution, and can favorably alter the
97 substratum electrode properties, such as surface roughness, conductivity and electrical
98 resistance. Wang et al [28] and Tasić et al. [29] have reported a Ni mesh with W
99 coating and a Au electrode with MoS, both of which exhibited high electrocatalytic
100 activities for hydrogen evolution. In addition, Mo(VI) can act as a catalysis for
101 co-deposition of W(VI) in conventional electrochemical processes [30-31].

102 In this study, stacked BESs composed of MFCs and MECs in multiple units with
103 serial and/or parallel connection, have been systematically investigated for the
104 deposition and separation of W(VI) and Mo(VI) with simultaneous production of
105 hydrogen. The performance of the stacked BESs was evaluated by linear sweep
106 voltammetry (LSV) and electrochemical impedance spectroscopy (EIS). The reaction
107 products deposited on the electrodes were analyzed by scannning electronic
108 microscopy (SEM), energy dispersive X-ray spectrometry (EDS), X-ray diffraction
109 (XRD) and X-ray photoelectron spectroscopy (XPS). The system parameters
110 including circuital current, W deposition (R_W), Mo deposition (R_{Mo}), separation factor

(ε), hydrogen production, cathodic (CE_{ca}) and anodic (CE_{an}) coulombic efficiencies, and overall system efficiency (η_{sys}) were extensively employed to assess system performance. The mutual effect of W(VI) and Mo(VI) species in solution, and the optimization of the stacked BESs have been investigated. This study provides an innovative approach for efficient deposition and separation of W(VI) and Mo(VI) with simultaneous hydrogen production, without the requirement of external energy input.

2 Materials and Methods

2.1 BES assembly

Identical dual-chamber BESs were used in all experiments, with the chambers separated by a cation exchange membrane (CMI-7000 Membranes International, Glen Rock, NJ). Porous graphite felts (1.0 × 1.0 × 1.0 cm, San ye Co., Beijing, China) were used as anodes, whereas stainless steel sheets (2.0 × 2.0 cm, Qing yuan Co., China) were used as cathodes. The stainless steel sheets were mechanically polished with abrasive papers and cleaned with ethanol and deionized water, before installation [32]. The operating volume of the anodic and cathodic chambers of each BES unit was 14 mL each.

Here Fig. 1

Nine operational BES configurations comprising a minimum of two and a maximum of six BES units were investigated as shown in Fig. 1, where BES-1-1 indicated two units in series, while BES-2-1, BES-3-1 and BES-4-1 represented two, three and four parallel units connected to a single unit in series, respectively. Similarly, the units in parallel were also serially connected with other parallel and single units,

134 respectively. For convenient expression, the reactor units in these modules were
135 denoted in order as 1#, 2# and 3# (Fig. 1). Derived from the concept of MFCs acting
136 as a power source and MECs requiring externally applied voltage (power input)
137 [33-34], the term of applied voltage was specifically used to illustrate that the 2# unit
138 of BES-3-1 acted as a driving force and a power to input voltage to the 1# unit,
139 similar to the previous description [20,22-25]. Data associated with 2# in the BES-3-1
140 have been shown as an average for the units connected in parallel since the differences
141 among the units were insignificant and for the sake of clarity. An external resistor of
142 10 Ω was used to collect the circuital current and the voltage output. A reference
143 electrode (Ag/AgCl, 195 mV vs. SHE) was installed in the cathodic chamber to
144 measure the cathodic potential, with all potentials reported here vs. SHE. All reactors
145 were wrapped with aluminum foil to ensure darkness, to avoid the growth of algae on
146 the anodes and possible side reactions on the cathodes.

147 *2.2 Inoculation and operation*

148 The anodes of the BES were inoculated with suspended bacteria from acetate-fed
149 anodes which were supplemented by an equivalent volume of anolyte solution, to
150 facilitate the acclimation of the anodic biofilms [21-22]. The composition of the
151 anolyte in deionized water was (g/L) sodium acetate 1.0; KH_2PO_4, 4.4; K_2HPO_4, 3.4;
152 NH_4Cl, 1.3; KCl, 0.78; $MgCl_2$, 0.2; $CaCl_2$, 0.0146; NaCl, 0.5; trace vitamins and
153 minerals [35]. The anolyte was sparged with ultrapure N_2 gas for 15 min to remove
154 residual oxygen, prior to transferring to the anodic chambers, whereas deionized water
155 was used as catholyte for anodic exoelectrogens acclimation [24-25]. The acclimation

process was carried out with an external resistor of 1000 Ω which was suitable for bacterial acclimation and avoided inaccurate assessment for subsequent power production [24-25,36-37]. The acclimation period was completed after eight anolyte refreshment cycles, when the anodic potential stabilized at –0.23 ~ –0.27 V vs. SHE, as shown in Fig.S1A. The reactor units were then stacked as shown in Fig. 1. The catholyte was replaced by a solution of Na_2WO_4 and Na_2MoO_4 (1.0 mM each) in deionized water, although the specific concentrations of these two metals in practical wastewaters may vary over a greater range of 0.05 ~ 10.4 mM [1-4]. The initial pH in the catholyte was set to 2.0 and the solution conductivity to 3.5 mS/cm, to reproduce the characteristics of acidic wastewaters containing W(VI) and Mo(VI) [1-3]. The acclimation of the all stacked BES units was completed after two further fed-batch cycle refreshments, which yielded reproducible electrode potentials in all BESs (every operation cycle lasted 4 h). Unless otherwise stated, the stainless steel cathodes were always cleaned in 1.0 M NaOH before each batch cycle operation.

The stability of the cells and the effect of pre-deposited W and Mo on the rate of hydrogen evolution were evaluated using the stacked BES-3-1 configuration, and considering a total of 20 fed-batch operation cycles, avoiding the cleaning of the cathodes. The bare electrodes, and the cathodes of 1# and 2# units in BES-3-1 after the 10^{th} and the 20^{th} operational cycle were analyzed by EIS. The catholyte effluent in the stacked BES-3-1 configuration was totally reused after pH adjustment to 2.5 and at constant solution conductivity (3.5 mS/cm), in order to achieve a higher W and Mo deposition and separation.

178 Control experiments using catholyte containing either W(VI) or Mo(VI) were
179 performed to evaluate the impact of using a mixture of these two metals on the system
180 performance. Further control experiments under open circuit conditions (OCCs)
181 reflected the effect of circuital current on the metals deposition. Other control
182 experiments using just the 1# unit or just the 2# unit of the BES-3-1 were performed
183 to illustrate the roles that each of these reactor units played on deposition of W and
184 Mo. All stacked reactors were operated in fed-batch mode at room temperature (25 ±
185 3 °C) and all experiments were conducted in duplicate. The inoculation and solution
186 replacements were performed in an anaerobic glove box (YQX-II, Xinmiao,
187 Shanghai).

188 *2.3 Measurements and analyzes*

189 W(VI) and Mo(VI) in the catholyte and chemical oxygen demand (COD) in the
190 anolyte were measured using standard methods [38]. The pH was measured by a
191 calibrated pH meter (PHS-3C, Leici, Shanghai) and solution conductivity was
192 measured using a conductivity meter (DDS-307, Leici, Shanghai). A glass tube with
193 an inner diameter of 8 mm was glued to the top of the cathodic chambers to create a
194 total headspace of 12 mL [32,39]. Hydrogen in the headspace of the cathodic
195 chambers was sampled using microsyringes (200 μL, Agilent) and analyzed by a gas
196 chromatograph (GC7900, Tianmei, Shanghai) which was equipped with a thermal
197 conductivity detector and a molecular sieve column (TDX-01, 60 – 80, 4 mm × 2 m).
198 The column operating temperature was 110 ºC and the injector and detector
199 temperatures were both 120 ºC. Argon was used as the carrier gas at a constant

200 pressure of 0.13 MPa [32,39]. Hydrogen production (m^3/m^3 d) was calculated from
201 the hydrogen concentration (m^3/m^3) obtained with the GC, multiplied by the gaseous
202 phase volume (m^3) and divided by the working volume (m^3) and operational time (d).
203 The morphologies of the electrodes after W and Mo deposition were examined
204 using a scanning electronic microscope (SEM) (QUANTA450, FEI company, USA)
205 equipped with an energy dispersive spectrometer (EDS) (X-MAX 20 mm^2/5- mm^2,
206 Oxford Instruments, UK). X-ray diffraction (XRD-6000, Shimadzu LabX, Japan) and
207 X-ray photoelectron spectroscopy (XPS, Kratos AXIS Ultra DLD) were used to
208 examine the nature and the elemental composition of the crystal products deposited on
209 the cathodes.
210 The cathode and anode potentials were monitored by an automatic data
211 acquisition system (PISO-813, Hongge Co, Taiwan). Polarization and power density
212 data were obtained with a potentiostat (CHI 760C, Chenhua, Shanghai) using linear
213 sweep voltammetry (LSV). Cyclic voltammetry (CV) (CHI 760C, Chenhua, Shanghai)
214 was carried out with a three-electrode configuration comprising a working electrode
215 (i.e, cathode), a platinum plate counter electrode, and a Ag/AgCl reference electrode.
216 CVs were conducted in solutions with either W(VI) or Mo(VI) species or with a
217 mixture of them, to reflect the reductive peak potentials and reductive peak currents of
218 W(VI) and Mo(VI) under the experimental condition. Both CV and LSV were
219 conducted at a scan rate of 1.0 mV/s. EIS was conducted using the same potentiostat
220 with a three electrode system comprising a working electrode (i.e., cathode), a
221 Ag/AgCl reference electrode (195 mV vs. SHE) located 1 cm away from the cathode

in the cathodic chamber, and a Pt foil (2 × 4 cm) counter electrode placed in the anodic chamber. Impedance analysis was conducted at cathode potentials under OCCs with either the bare electrodes, or the electrodes deposited with W and Mo (obtained after multiple batch cycle operations) in catholyte to determine the impact of the W and Mo deposits on the subsequent W(VI) and Mo(VI) reduction in the stacked BES-3-1. For assessment of effect of W and Mo deposits on subsequent hydrogen evolution, however, impedance analysis was carried out at cathode potentials under CCCs with the same electrodes mentioned above but using catholyte in the absence of W(VI) and Mo(VI). EIS frequency ranged from 100 kHz to 10 mHz, with a sinusoidal perturbation of 10 mV amplitude. The equivalent circuits and detailed values of different resistances were obtained through Zsimpwin software and normalized to the projected area of the cathodes [40-41].

The statistical significance of the experimental data was assessed using a statistical package (SPSS v.19.0) (t-test, $p = 0.05$).

2.4 Calculation

W deposition (R_W, %) and Mo deposition (R_{Mo}, %) were calculated from Eqs. 1 – 2. The power density was normalized to the projected surface area of the separator, allowing the comparison of the results to literature studies based on power per unit area [18,24,42]. The CE_{an}, CE_{ca}, and η_{sys} were calculated from Eqs. 3 – 8 [21] whereas the ε was directly related with R_W and R_{Mo}, and calculated from Eq. 9 [1,8]:

$$R_W = \frac{W(VI)_0 - W(VI)_t}{W(VI)_0} \times 100\% \quad (1)$$

$$R_{Mo} = \frac{Mo(VI)_0 - Mo(VI)_t}{Mo(VI)_0} \times 100\% \quad (2)$$

$$Y_W = \frac{(W(VI)_0 - W(VI)_t) \times V_{ca} \times 32}{(COD_0 - COD_t) \times V_{an}} \quad (3)$$

$$Y_{Mo} = \frac{(Mo(VI)_0 - Mo(VI)_t) \times V_{ca} \times 32}{(COD_0 - COD_t) \times V_{an}} \quad (4)$$

$$Y_{H_2} = \frac{\eta_{H_2} \times V_{H_2} \times 32}{(COD_0 - COD_t) \times V_{an}} \quad (5)$$

$$CE_{an} = \frac{\int_0^t Idt}{96485 \times \frac{4 \times (COD_0 - COD_t) \times V_{an}}{32}} \times 100\% \quad (6)$$

$$CE_{ca} = \frac{[b_1 \times (W(VI)_0 - W(VI)_t) \times V_{ca} + b_2 \times (Mo(VI)_0 - Mo(VI)_t) \times V_{ca} + b_3 \times \eta_{H_2} \times V_{ca}] \times 96485}{\int_0^t Idt} \times 100\% \quad (7)$$

$$\eta_{sys} = \frac{b_1 \times (W(VI)_0 - W(VI)_t) \times V_{ca} + b_2 \times (Mo(VI)_0 - Mo(VI)_t) \times V_{ca} + b_3 \times \eta_{H_2} \times V_{ca}}{(COD_0 - COD_t) \times V_{an} \times \frac{4}{32}} \times 100\% \quad (8)$$

$$\varepsilon = \frac{Mo(VI)_0 - Mo(VI)_t}{Mo(VI)_0} \times \frac{W(VI)_t}{W(VI)_0 - W(VI)_t} = \frac{1 - R_W}{R_W} \times \frac{R_{Mo}}{1 - R_{Mo}} \quad (9)$$

where $W(VI)_0$, $Mo(VI)_0$ and COD_0 are the initial concentrations (mol/L) of W(VI) and Mo(VI) in the catholyte, and of COD in the anolyte of each unit, respectively, and the subscript t refers to the concentration after an operational time of t (h). η_{H2} is the hydrogen concentration (mol/L) at t hours; V_{ca} and V_{an} are the volumes of liquid (L) in the cathodic and anodic chambers, respectively; I is the corresponding circuital current (A); 96485 is the Faraday constant (C/mol e^-); 4 is the molar number of electrons required for oxygen reduction (mol/mol); 32 is the atomic weights of O_2

(g/mol); b_1, b_2 and b_3 are the molar numbers of electrons required for W(VI) and Mo(VI) reduction, and for hydrogen evolution (mol/mol).

3 Results and discussion

3.1 Performance of stacked BES-3-1 configuration

Here Fig. 2

Here Table 1

W and Mo were deposited more efficiently in the stacked BES-3-1 configuration, achieving 27.6 ± 1.2% for W with a yield of 0.09 ± 0.01 mol/mol COD (Fig. 2A and Table 1) and 75.4 ± 2.1% for Mo with 0.26 ± 0.02 mol/mol COD (Fig. 2B and Table 1) in the 1# unit, and 12.3 ± 0.9% with 0.08 ± 0.01 mol/mol COD (W) (Fig. 2A and Table 1) and 52.6 ± 2.2% with 0.23 ± 0.01 mol/mol COD (Mo) (Fig. 2B and Table 1) in the 2# unit. Accordingly, higher CE_{an} of 52 ± 1% in the 1# unit than 42 ± 3% in the 2# unit (p = 0.013), and similar CE_{ca} of 70 ± 5% (1#) and CE_{ca} of 67 ± 1% (2#) (p = 0.15) (Table 1) were observed. These results reflect the higher reductive environment in the 1# unit due to the lower cathode potential (average values in Fig. 2C; as a function of time in Fig. S1B), the higher circuital current (average values in Fig. 2D; as a function of time in Fig. S1B), and the impact of the voltage output from the 2# unit (MFC) which was applied to the 1# unit (MEC) (Fig. 2E).

While the CE_{an} were somewhat lower than values reported for single BES units, particularly those utilizing high efficient Pt-cathodes [33,37], the overall system efficiencies (η_{sys}) were equivalent, and in some cases even higher, to MFC-MEC utilizing graphite granule anodes and cathodes, using $K_3Fe(CN)_6$ and methyl orange as cathodic electron acceptor, respectively [20]. The η_{sys} was slightly lower than in

285 MFC-MEC with carbon paper anodes and Pt catalyzed cathodes using oxygen and H^+
286 as cathodic electron acceptor, respectively [19]. The different CE_{an} observed in the 1#
287 and 2# units reflect the existence of different microbial communities, consistent with
288 the corresponding different circuital currents (Fig. 2D). In fact, circuital current is
289 well known to influence microbial community in BESs [33]. Various strategies could
290 be adopted to further increase the CE_{an}, such as through dosing of chemical methane
291 inhibitors (e.g. 2-bromo-ethanesulfonate) [43] or by decreasing the anodic cycle
292 time/hydraulic retention time, to inhibit methane production [44], which subsequently
293 could enhance the amount of cathodic electrons used for the deposition of W and Mo
294 in the stacked BESs.

295 Under the experimental condition, W(VI) and Mo(VI) reductions occurred at
296 potentials more positive than -0.042 V (Fig. S2), which were more positive than the
297 potentials of the cathodes in the 1# and 2# units (Fig. 2C and S1B), confirming the
298 presence of favorable reductive environments in both units of the stacked BES-3-1.
299 The co-existence of W(VI) and Mo(VI) in solution yielded higher reductive peak
300 currents in comparison to the cases with individual metal salts (Fig. S2), illustrating
301 the dual benefits of W(VI) and Mo(VI) for the occurrence of reduction reactions.

302 In the control experiments with either the 1# or 2# unit, the amount of W and Mo
303 deposition was 15.3 ± 1.7% (p = 0.000) and 60.1 ± 1.6% (p = 0.000) (1#), and 12.9 ±
304 1.3% (p = 0.864) (W) and 56.1 ± 2.0% (p = 0.134) (Mo) (2#), respectively (Fig. S3),
305 reflecting that the 2# unit positively affected the performance of 1# unit, whereas the
306 1# unit negligibly influenced the performance of 2# unit in the stacked BESs. In the

control experiments using catholytes with either W(VI) or Mo(VI), the deposition of W was 6.8 ± 1.3% (1#, p = 0.000) and 3.3 ± 0.4% (2#, p = 0.000) (Fig. 2A) and the deposition of Mo was 65.1 ± 3.2% (1#, p = 0.013) and 45.2 ± 0.9% (2#, p = 0.014) (Fig. 2B), consistent with the results in Fig. S2, reflecting again the dual benefits of W(VI) and Mo(VI) for efficient co-deposition in the stacked BESs. This effect has also been observed in conventional electrochemical processes [30-31]. Note that under OCCs, only 2.9% of W and Mo was deposited, with the single metals and with a mixture of the two metals. A control experiment with only anolyte in the absence of the electrode and exoelectrogens was specifically performed to evaluate the rate of diffusion of W(VI) and/or Mo(VI) from the cathodic to the anodic chambers under OCCs. In parallel, the morphology of the deposits on the cathode electrode was analyzed with SEM-EDS to ascertain the presence of W and/or Mo. The results showed that after a fed batch cycle, the concentrations of W and/or Mo in the anolyte were undetectable, excluding the possibility of W and/or Mo diffusion from the cathode to the anode, although the retention of W and/or Mo on the ion exchange membrane could not be precluded. The detection of W and Mo on the cathode electrode (Fig. S4) confirmed the occurrence of adsorption of W and Mo on the cathode.

Simultaneous with the W(VI) and Mo(VI) co-deposition process, the production of hydrogen in the 1# unit was 0.34 ± 0.01 m^3/m^3 d with a yield of 0.87 ± 0.03 mol/mol COD, compared to the rates obtained with the single metals in the control experiments (0.29 ± 0.00 m^3/m^3 d with Mo(VI) alone (p = 0.193) and 0.15 ± 0.01

329 m^3/m^3 d with W(VI) alone (p = 0.012)) (Fig. 2F and Table 1). The rate of hydrogen
330 production in the 1# unit of the stacked BES-3-1 was higher than literature results
331 using titanium sheet platinum-coated cathodes in MECs operated at a pH of 6.0 and
332 temperature of 55 ºC (0.2 – 0.3 m^3/m^3 d) [45-46], and was comparable to the rates
333 obtained with the same platinum sheet metal cathodes of MECs at a high applied
334 voltage of 0.9 V but neutral pH (0.68 m^3/m^3 d) [47]. The production of hydrogen in
335 BESs is significantly affected by solution pHs [48]. Taken together with the
336 requirements of H^+ for W(VI) and Mo(VI) reduction as well as hydrogen evolution in
337 the stacked BESs (Eqs. S1-S5), a cathodic pH maintained at 2.0 should favor the
338 highest rate of hydrogen production [48]. As an example, the electron distribution in
339 the stacked BES-3-1 after one batch cycle operation is shown schematically in Fig.
340 S5.

341 The metal separation factors in the 1# and 2# units were similar (8.1 ± 0.2 and
342 7.9 ± 0.5, respectively, p = 0.465) (Table 1), which were higher than the value (7.0)
343 reported with a macroporous resin or using manganese dioxide as adsorbent [6,8].
344 They were also equivalent to the separation factor obtained with $MnSO_4$ as a
345 precipitation reagent [1-2] at the same W(VI) and Mo(VI) concentrations. However,
346 the metal separation factors were lower than those reported with commercial TEVA or
347 macroporous resins (from 14 to 28) at a ratio of W(VI) and Mo(VI) of 1 : 20, and the
348 separation factor of 105, reported using solvent extraction with H_2O_2 as a chelating
349 agent [2,6-7].

350 **Here Fig. 3**

The polarization curves with the W(VI) and Mo(VI) mixture (Fig. 3A) were similar to those observed in the control experiments with Mo(VI) alone (Fig. 3C), with maximum power higher than with W(VI) alone (Fig. 3E). These results clearly demonstrate the greater importance of Mo(VI) than W(VI) for delivering maximum power production. Accordingly, the power production in the control experiments with either the 1# or 2# unit (Fig. 3A) reflected more favorably the 2# unit rather than the 1# unit, elucidating that the 2# unit acted as MFCs and that the 1# unit acted as MECs, in the stacked BESs.

The cathodic potentials varied more significantly than the anodic potentials over the current density range (Fig. 3B). Similarly, an increase in current density in the control experiments with either the 1# or 2# unit resulted in more rapid gradients in the cathodic rather than in the anodic potentials (Fig. 3B). These results imply that the performance of the stacked BESs, as well as, each of the 1# and 2# units was augumented by changes in the cathode properties. These results are supported by the increasing consensus that BES performance may be constrained by poor reaction kinetics at the cathode, which results from the complex catholyte composition used and the subsequent multiple competitive reactions that may be generated, the accumulation of OH^- and other products near to the cathode surface and the cathode overpotential [9,49]. The cathode potentials as a function of current density in the controls with Mo(VI) alone (Fig. 3D), decreased more significantly than those obtained with W(VI) alone (Fig. 3F), stressing the greater importance of Mo(VI) rather than W(VI) for determining the cathode potential, consistent with the results in

373 Fig. 2A and B.

374 *3.2 Electrode morphology and product analysis*

375 Products with a smaller area of blue color (Fig. 4A) and with more club-shaped
376 agglomerates (Fig. 4E) were observed in the layer deposited on the cathode of the 1#
377 unit, compared to those observed on the 2# unit (Fig. 4B and F) or on the bare
378 electrode (Fig. S6). The observation of a blue color implies a small amount of reduced
379 Mo and W on the cathodes [1]. The exposure of the deposits to air led to substantial
380 changes in the color (Fig. 4C and D) and microscopic morphology (Fig. 4G and H) in
381 both the 1# (Fig. 4C and G) and 2# units (Fig. 4D and H), implying the sensitivity of
382 the deposits to oxygen. Although the size and shape of the particles deposited on the
383 cathodes were not tightly controlled, the variety of the morphologies observed on
384 these cathodes implies that the different units in the stacked BES-3-1 produced
385 products with different morphologies.

386 EDS analysis of the agglomerates in the deposits of the 1# unit reported higher
387 W (at binding energies of 1.60, 1.78, 8.40 and 9.70 keV) and Mo (at 2.28 keV) signals
388 (Fig. 4I), compared to those observed in the 2# unit (Fig. 4J), confirming the higher
389 efficiency of the 1# unit for metal deposition (Fig. 2A and B). The W content in the
390 products was 2.68% (1#) and 0.67% (2#), well below the 5 – 6% range usually
391 leading to the formation of cracked W and Mo surface [30,50], consistent with the
392 SEM observation in Fig. 4E and F. Exposure to air led to a decrease of the W and Mo
393 signals in both the 1# (Fig. 4K) and 2# units (Fig. 4L), mainly ascribed to the fast
394 oxidation of these reduced products [2,5,30]. The observation of Fe, Cr, Mn, Ni, C

and O on all the cathodes was associated with the composition of the stainless steel substratum. The XRD patterns closely matched $Mo_{8.8}W_{1.2}O_{29}$ (–404) at 24.4° and (302) at 29.7°, and MoO_2 (010) at 63.4° and (102) at 68.7° in the 1# unit (Fig. 4M and Table S1), compared to $Mo_{9.35}W_{1.65}O_{32}$ (–203) at 21.8°, (301) at 25.7° and (–501) at 25.9°, and MoO_2 (404) at 60.9° and (110) at 68.9° in the 2# unit (Fig. 4N and Table S1). Exposure to air completely changed the forms of the crystals in both the 1# (Fig. 4O) and 2# units (Fig. 4P). In concert, the results observed support a significant dependence of the product crystals on the variety of units in the stacked BES-3-1 and that the products were highly sensitive to oxidation.

Here Fig. 5

XPS images displayed the presence of peaks at 35.9 and 38.1 eV for W on all the electrodes (Fig. 5A, C, E and G), which were assigned to W(VI) at W(4f7/2) and W(4f5/2) levels, respectively. However, this could not preclude the oxidation of the highly unstable W(V) as a reduced product during the sample preparation [2,5,30]. In fact, electrodes sampled at the end of one operational cycle, in the absence of N_2 protection, instantly changed in color, implying the weak oxidative character of anionic polymerized W(VI). Accordingly, higher peaks at 234.8 eV and 231.8 eV associated with Mo(V) than those at 231.0 eV and 234.0 eV assigned to Mo(IV) were observed in the 1# unit, both of which were higher than those in the 2# unit (Fig. 5B and Table S2), consistent with the results in Fig. 2B. The reduction of Mo(VI) to Mo(V) was therefore more likely than the reduction towards Mo(IV).

3.3 BESs stacked in different configurations

Here Fig. 6

418 Among the various configurations of stacked BESs, BES-4-1 comprising a single
419 unit (1#) serially connected with four parallel units (2#) (Fig. 1) exhibited the similar
420 highest deposition of metals to BES-3-1 in the same 1# unit: 28.7 ± 0.7% (W) (p =
421 0.528) (Fig. 6A) and 69.1 ± 1.3% (Mo) (p = 0.15) (Fig. 6B). In the 2# unit, however,
422 Mo deposition of 39.3 ± 1.7% in BES-4-1 (Fig. 6B) was lower than 52.6 ± 2.2% in
423 BES-3-1 (p = 0.042) (Fig. 2B), compared to the similar W deposition (13.2 ± 1.6% in
424 BES-4-1, 12.3 ± 0.9% in BES-3-1, p = 0.684). As a consequence, separation factor of
425 4.3 ± 0.1 in the 2# unit of BES-4-1 was significantly lower than 7.9 ± 0.5 in BES-3-1
426 based on Eq. 9 (Table 1). While hydrogen production of 0.83 ± 0.20 m^3/m^3 d in
427 BES-4-1 was higher than 0.34 ± 0.10 m^3/m^3 d in BES-3-1 (Table 1), the yield of
428 hydrogen in BES-4-1 (0.56 ± 0.01 mol/mol COD) was lower than in BES-3-1 (0.87 ±
429 0.03 mol/mol COD), explained by the higher rate of COD consumption in the
430 BES-4-1 anode, according to Eq. 5. Taken together, BES-4-1 had an advantage of
431 more hydrogen production over BES-3-1 whereas the latter favored for more Mo
432 deposition and the subsequent more efficient W and Mo separation. Considering the
433 merit of favor for more metal deposition and separation in BES-3-1, this stacked
434 BES-3-1 module was thus selected to evaluate the effect of multiple cycles operation,
435 and the effect of effluent reuse from the 1# and 2# units, for complete separation of W
436 from Mo.

437 It should be noted that each of these reactor units could independently generate
438 current prior connection in stacked BESs. BES-2-1, BES-3-1 and BES-4-1 modules
439 were made of MECs (1#) and MFCs (2#, associated two, three or four units in a

parallel connection). These stacked systems operated spontaneously at voltage outputs higher than that from coupled single units (1#), since the internal resistance, in the parallel connected units, progressively decreased as the number of parallel connected units increased. Therefore, at a fixed external resistance (e.g. 1#), the stacked BESs would spontaneously evolve hydrogen, as long as the voltage output from the units connected in parallel (e.g. 2#) could produce a more negative cathodic potentials in the 1# unit, sufficient for H^+ reduction (theoretically –0.135 V at the present initial pH of 2.0) [34]. The hydrogen production rate, however, dynamically depended on the circuital current of the BESs [34]. Thus, hydrogen was thermodynamically evolved in the 1# unit rather than the 2# unit, evolving a higher hydrogen production rate in BES-4-1 rather than in BES-3-1 (Fig. 2C and 6C, Table 1). However, the inadequate cathodic potential and circuital currents in the 1# unit of BES-2-1 resulted in negligible evolution of hydrogen (Table 1 and Fig. 6C and 6D). In BES-3-2-1, the three units connected in parallel acted as MFCs, while the two units in parallel serially stacked with a single unit, served as MECs. The hydrogen production in BES-3-2-1 was reasonably lower than the 1# unit of BES-3-1 due to the more number of units being driven in the former (Table 1). The BESs with equal number of serial and/or parallel connected units including BES-1-1, BES-2-2, BES-3-3, BES-1-1-1 and BES-2-2-2, produced similar voltage outputs and net electricity was always produced, excluding the possibility of hydrogen evolution in these systems.

3.4 BES long-term stability

Here Fig. 7

The deposition of W in both the 1# and 2# units of the BES-3-1 exhibited a

463 decreasing trend with operational time, from 27.6 ± 1.2 % (1#) and 12.3 ± 0.9 % (2#)
464 in the first cycle to 10.1 ± 1.3% (1#) and 8.4 ± 0.8% (2#) after the 20th cycle (Fig. 7A).
465 Conversely, Mo deposition in the 2# unit gradually increased, from the initial 52.6 ±
466 2.2% (1st cycle) to 61.6 ± 2.2% (20th cycle) (Fig. 7B). The insignificant change in the
467 deposition of Mo in the 1# unit (71.7 – 75.4%) was accompanied with an increase in
468 hydrogen production (Table S3), reflecting the beneficial catalytic effect of the Mo
469 deposit on hydrogen evolution [29]. Specifically, it has been shown that MoS_2
470 particles coated carbon cloth performs better than bare stainless steel and even
471 surpasses platinum-based electrodes for hydrogen evolution [51].

472 The separation factor in BES-3-1 increased from 8.1 ± 1.4 (1#) and 7.9 ± 0.0 (2#)
473 (1st cycle) to 22.8 ± 1.9 (1#) and 17.7 ± 0.8 (2#) (20th cycle) (Fig. 7C), suggesting a
474 beneficial effect of the operational time on the separation of the metals.

475 Cathode potentials (Fig. 7D), circuital current (Fig. 7E), applied voltage (Fig.
476 7F) and hydrogen production (Table S3) increased progressively up to a maximum at
477 the 10th cycle, which were consistent with the polarization curves (Fig. S8) and with
478 the appreciable deposition of W and Mo on the electrodes (Fig. 7A and B). Such
479 results are further supported by the positive effect of tungsten and molybdenum oxide
480 impregnated electrodes in MFCs for power production and V(V) or O_2 reduction
481 [52-54]. Further deposition of the metals from the 11th to 20th cycle, resulted in a
482 decrease in the circuital current (Fig. 7E) and negligible changes in the cathode
483 potential (Fig. 7D), which ultimately led to a decrease of the hydrogen production
484 with operational time (Table S3). This last effect could be attributed to an excessive

accumulation of metals on the electrodes, which was further proved as follows.

The EIS spectra were fitted to equivalent circuits (Fig. S9) to identify the components determining the internal resistances in the BES-3-1 after the 10^{th} and 20^{th} cycle, for assessing W(VI) and Mo(VI) reduction, and hydrogen evolution (Fig. S10 and Table S4) in comparison with the bare electrodes. The diffusional resistance (R_d) for W(VI) and Mo(VI) reduction was significantly higher than the polarization (R_p) and the ohmic (R_o) resistances (Fig. S10A and Table S4) due to the mass transfer limitation of the formed macromolecules of W and Mo heteropolyacid [1-2]. Compared to the bare electrode, the R_d, R_p and R_o resistances after the 10^{th} cycle substantially decreased to 4252.3 Ω, 43.2 Ω and 14.8 Ω (1#) and 2076.7 Ω, 25.4 Ω and 14.2 Ω (2#), respectively, which were consistent with the enhanced system performance due to the presence of W and Mo deposits (Fig. 7). However, at the 20^{th} cycle, R_d and R_p increased, while R_o negligibly changed, which was attributed to the excessive W and Mo layer formed.

With respect to the bare electrode having R_p of 89.4 Ω, R_d of 4897.2 Ω and R_o of 18.2 Ω for hydrogen evolution (Fig. S10B and Table S4), the rate of hydrogen production increased after a prolonged operation (10^{th} cycle) (Table S3) due to the decrease of the resistance, R_p (22.7 Ω), R_d (503.5 Ω) and R_o (7.3 Ω). However, further use (20^{th} cycle) led to an increase in the resistances, R_p (43.4 Ω), R_d (1123.4 Ω) and R_o (10.5 Ω) (Table S4) and, in consequence, to a decrease in the rate of hydrogen production (Table S3), consistent with the EIS results for W(VI) and Mo(VI) reduction (Fig. S10A and Table S4). These results, in concert, clearly demonstrated

507 that the decreased rate of hydrogen production at the 20th cycle resulted from the
508 excessive layer of W and Mo built on the cathodes of 1# in the stacked BESs.

509 *3.5 Catholyte effluent reuse*

510 The catholyte effluent after acidic adjustment was fully reused in the BES-3-1
511 to increase the amount of metal deposited, which reached 36.0 ± 0.3% (W) and 99.4 ±
512 0.5% (Mo) in the 1# unit, and 26.9 ± 0.2% (W) and 96.2 ± 0.6% (Mo) in the 2# unit at
513 the 7th circulation (Fig. S11A and B). Accordingly, a significantly higher separation
514 factor equal to 467 ± 22 was reached in the 1# unit, compared to 70 ± 3 in the 2# unit
515 (Fig. S11C). This separation factor achieved in the 1# unit was higher than that
516 observed with ion exchange resins, solvent extraction, or MnO_2 and $MnSO_4$
517 adsorbents (range 7 – 105) [2,6-8]. A decrease of the concentration of W(VI) and
518 Mo(VI) in the catholyte with reuse led to a decrease of the circuital current (Fig.
519 S11D), the cathode potential (Fig. S11E), and the applied voltage to the 1# unit (Fig.
520 S11F) as expected, due to the progressive reduction of W(VI) and Mo(VI) electron
521 acceptors in the catholyte. This result was consistent with the reports using other
522 multiple metals as electron acceptors in BESs [17-18,55-56]. The pH of the catholyte
523 after each reuse always increased in both the 1# (Fig. S11G) and the 2# unit (Fig.
524 S11H), and required a pre-acidification step to promote efficient W and Mo deposition
525 and separation.

526 On the basis of the operating costs alone, the net value of W and Mo products
527 recovered from the system (7.22 $ per m^3 mixed W(VI) and Mo(VI)) was significantly
528 higher than the cost required for acidification of the catholyte (0.03 $/$m^3$),

529 demonstrating the economical feasibility of this technology.

530 With regard to the practical application of stacked BESs for W and Mo recovery,
531 the two-chamber BESs have merits over the one-chamber systems, since these avoid
532 the toxicity of W and Mo to the anodic exoelectrogens while permitting the
533 simultaneous treatment of two different wastewaters [9-10]. Considering that the
534 materials costs are steadily decreasing, particularly the costs of the ion exchange
535 membrane [27,42,55,57], cost-effective two-chamber stacked BESs are promising
536 systems for sustainable recovery and separation of W and Mo at industrial scale, with
537 simultaneous production of hydrogen. However, the practical implementation of this
538 technology for industrial wastewater treatment requires further pilot and full-scale
539 investigations, to evaluate the long-term operation and stability of the system over
540 feeds with fluctuating characteristics [57]. In addition, in this study we have adjusted
541 the pH to the acidic value of 2.0 only at the beginning of the experiment, although a
542 recent study suggests that a pH control during the entire operational period to acidic
543 values may lead to enhanced performance [48]. This aspect should be investigated in
544 further studies. The separation of the W and Mo layer deposited on the electrodes may
545 also represent a further challenge for the practical application of this technology.
546 However, the in-situ utilization of these deposits for photocatalytic processes may
547 become an attractive strategy for reuse, since W and Mo oxides exhibits excellent
548 photocatalytic properties [58]. It is expected that further optimization of pH control,
549 and ratio of W(VI) and Mo(VI) would result in an improved performance of the
550 stacked BESs presented in this study.

4 Conclusions

This study demonstrated a novel method for the deposition and separation of W and Mo metals in stacked BESs with simultaneous hydrogen production, without the need of external energy input. The optimized stacked module was the BES-3-1, where the dual benefits of the W(VI) and Mo(VI) species, and the favorable impact of the 2# unit on the 1# unit were observed, with simultaneous hydrogen production. This system also displayed a favorable configuration in which the 2# MFC unit assisted the 1# MEC unit. Further reuse of the catholyte after acidification led to complete separation of W and Mo from one another. Since W(VI) and Mo(VI) are extensively present in ore dressing wastewater, this study may provide a sustainable and environmentally benign approach to this industry for efficient recovery and separation of W and Mo with simultaneous hydrogen production.

Acknowledgments

The authors gratefully acknowledge financial support from the National Natural Science Foundation of China (No. 51578104), and the Programme of Introducing Talents of Discipline to University (B13012).

References

[1] Z. Zhao, C. Cao, X. Chen, G. Huo, Separation of macro amounts of tungsten and molybdenum by selective precipitation, Hydrometallurgy 108 (2011) 229-232.

[2] T.A. Lasheen, M.E. El-Ahmady, H.B. Hassib, A.S. Helal, Molybdenum metallurgy review: hydrometallurgical routes to recovery of molybdenum from ores and mineral raw materials, Mineral Processing Extractive Metall. Rev. 36 (2015) 145-173.

[3] T. Ogi, T. Makino, K. Okuyama, W.J. Stark, F. Iskandar, Selective biosorption and

recovery of tungsten from an urban mine and feasibility evaluation, Ind. Eng. Chem. Res. 55 (2016) 2903-2910.
[4] P. Nekovář, Schrötterová, Extraction of V(V), Mo(VI) and W(VI) polynuclear species by primene JMT, Chem. Eng. J. 79 (2000) 229-233.
[5] B.P. Hahn, K.J. Stevenson, Cathodic electrodeposition of mixed molybdenum-selenium oxides, J. Electroanal. Chem. 638 (2010) 151-160.
[6] W.J. Guan, G.Q. Zhang, L.S. Xiao, D.Z. Wang, Continuous running test of the solvent extraction separation of Mo and W by H_2O_2-complexation with TRPO/TBP, Hydrometallurgy 157 (2015) 1-8.
[7] W. Zhang, J. Li, Z. Zhao, S. Huang, X. Chen, K. Hu, Recovery and separation of W and Mo from high-molybdenum synthetic scheelite in HCl solutions containing H_2O_2, Hydrometallurgy 155 (2015) 1-5.
[8] Y. Song, X. Chen, Z. Zhao, J. Zhang, L. He, Theoretical basis for the separation of W and Mo with manganese dioxide: a speciation-based approach, Metall. Mater. Trans. B. 47B (2016) 675-685.
[9] H. Wang, Z.J. Ren, Bioelectrochemical metal recovery from wastewater: a review, Water Res. 66 (2014) 219-232.
[10] Y.V. Nancharaiah, S.V. Mohan, P.N.L. Lens, Biological and bioelectrochemical recovery of critical and scarce metals, Trend Biotechnol. 34 (2016) 137-155.
[11] S.M. Iskander, B. Brazil, J.T. Novak, Z. He, Resource recovery from landfill leachate using bioelectrochemical systems: Opportunities, challenges, and perspectives, Bioresour. Technol. 201 (2016) 347-354.
[12] L. Huang, R. Guo, L. Jiang, X. Quan, G. Chen, Cobalt leaching from lithium cobalt oxide in microbial electrolysis cells, Chem. Eng. J. 220 (2013) 72-80.
[13] B. Zhang, C. Feng, J. Ni, J. Zhang, W. Huang, Simultaneous reduction of vanadium (V) and chromium (VI) with enhanced energy recovery based on microbial fuel cell technology, J. Power Sources 204 (2012) 34-39.
[14] O. Modin, X. Wang, X. Wu, S. Rauch, K.K. Fedje, Bioelectrochemical recovery of Cu, Pb, Cd, and Zn from dilute solutions, J. Hazard. Mater. 235-236 (2012) 291-297.
[15] H. Tao, T. Lei, G. Shi, X. Sun, X. Wei, L. Zhang, W. Wu, Removal of heavy metals from fly ash leachate using combined bioelectrochemical systems and electrolysis, J. Hazard. Mater. 264 (2014) 1-7.
[16] H. Luo, G. Liu, R. Zhang, Y. Bai, S. Fu, Y. Hou, Heavy metal recovery combined with H-2 production from artificial acid mine drainage using the microbial electrolysis cell, J. Hazard. Mater. 270 (2014) 153-159.
[17] Q. Wang, L. Huang, Y. Pan, P. Zhou, X. Quan, B.E. Logan, H. Chen, Cooperative cathode electrode and in situ deposited copper for subsequent enhanced Cd(II) removal and hydrogen evolution in bioelectrochemical systems, Bioresour. Technol. 200 (2016) 565-571.
[18] L. Huang, Q. Wang, L. Jiang, P. Zhou, X. Quan, B.E. Logan, Adaptively evolving bacterial communities for complete and selective reduction of Cr(VI), Cu(II) and Cd(II) in biocathode bioelectrochemical systems, Environ. Sci. Technol. 49 (2015) 9914-9924.

[19] M. Sun, G. Sheng, L. Zhang, C. Xia, Z. Mu, X. Liu, H. Wang, H. Yu, R. Qi, T. Yu, M. Yang, An MEC-MR-coupled system for biohydrogen production from acetate, Environ. Sci. Technol. 42 (2008) 8095-8100.
[20] Y. Li, H. Yang, J. Shen, Y. Mu, H. Yu, Enhancement of azo dye decolourization in a MFC-MEC coupled system, Bioresour. Technol. 202 (2016) 93-100.
[21] L. Huang, B. Yao, D. Wu, X. Quan, Complete cobalt recovery from lithium cobalt oxide in self-driven microbial fuel cell - microbial electrolysis cell systems, J. Power Sources 259 (2014) 54-64.
[22] Y. Zhang, L. Yu, D. Wu, L. Huang, P. Zhou, X. Quan, G. Chen, Dependency of simultaneous Cr(VI), Cu(II) and Cd(II) reduction on the cathodes of microbial electrolysis cells self-driven by microbial fuel cells, J. Power Sources 273 (2015) 1103-1113.
[23] J. Shen, Y. Sun, L. Huang, J. Yang, Microbial electrolysis cells with biocathodes and driven by microbial fuel cells for simultaneous enhanced Co(II) and Cu(II) removal, Front. Environ. Sci. Eng. 9 (2015) 1084-1095.
[24] D. Wu, Y. Pan, L. Huang, X. Quan, J. Yang, Comparison of Co(II) reduction on three different cathodes of microbial electrolysis cells driven by Cu(II)-reduced microbial fuel cells under various cathode volume conditions, Chem. Eng. J. 266 (2015) 121-132.
[25] D. Wu, Y. Pan, L. Huang, P. Zhou, X. Quan, H. Chen, Complete separation of Cu(II), Co(II) and Li(I) using self-driven MFCs-MECs with stainless steel mesh cathodes under continuous flow conditions, Sep. Purif. Technol. 147 (2015) 114-124.
[26] M. Li, Y. Pan, L. Huang, Y. Zhang, J. Yang, Continuous flow operation with appropriately adjusting composites in influent for recovery of Cr(VI), Cu(II) and Cd(II) in self-driven MFC-MEC system, Environ. Technol. 38 (2017) 615-628.
[27] X. Chen, P. Liang, X. Zhang, X. Huang, Bioelectrochemical systems-driven directional ion transport enables low-energy water desalination, pollutant removal, and resource recovery, Bioresour. Technol. 215 (2016) 274-284.
[28] T. Wang, L. Liu, Z. Zhu, P. Papakonstantinou, J. Hu, H. Liu, M. Li, Enhanced electrocatalytic activity for hydrogen evolution reaction from self-assembled monodispersed molybdenum sulfide nanoparticles on an Au electrode, Energy Environ. Sci. 6 (2013) 625-633.
[29] G.S. Tasić, U. Lačnjevac, M.M. Tasić, M.M. Kaninski, V.M. Nikolić, D.L. Žugić, V.D. Jović, Influence of electrodeposition parameters of Ni-W on Ni cathode for alkaline water electrolyser, Inter. J. Hydrogen Energy 38 (2013) 4291-4297.
[30] S. Sun, T. Bairachna, E.J. Podlaha, Induced codeposition behavior of electrodeposited NiMoW alloys, J. Electrochem. Soc. 160 (2013) D434-D440.
[31] F. Jiang, Y. Zhang, N. Sun, J. Leng, Tungsten coating prepared on molybdenum substrate by electrodeposition from molten salt in air atmosphere, Appl. Surf. Sci. 327 (2015) 432-436.
[32] Q. Wang, L. Huang, H. Yu, X. Quan, Y. Li, G. Fan, L. Li, Assessment of five different cathode materials for Co(II) reduction with simultaneous hydrogen evolution in microbial electrolysis cells, Inter. J. Hydrogen Energy 40 (2015)

665 184-196.
666 [33] B.E. Logan, Essential data and techniques for conducting microbial fuel cell and
667 other types of bioelectrochemical system experiments, ChemSusChem 5 (2012)
668 988-994.
669 [34] A. Kadier, M.S. Kalil, P. Abdeshahian, K. Chandrasekhar, A. Mohamed, N.F.
670 Azman, W. Logroño, Y. Simayi, A.A. Hamid, Recent advances and emerging
671 challenges in microbial electrolysis cells (MECs) for microbial production of
672 hydrogen and value-added chemicals. Renew Sust Energ Rev 61 (2016) 501-525.
673 [35] L. Huang, L. Gan, N. Wang, X. Quan, B.E. Logan, G. Chen, Mineralization of
674 pentachlorophenol with enhanced degradation and power generation from air
675 cathode microbial fuel cells, Biotechnol. Bioeng. 109 (2012) 2211-2221.
676 [36] Z.Y. Ren, H.J. Yan, W. Wang, M.M. Mench, J.M. Regan, Characterization of
677 microbial fuel cells at microbially and electrochemically meaningful time scales,
678 Environ. Sci. Technol. 45 (2011) 2435-2441.
679 [37] W. Yang, K.Y. Kim, P.E. Saikaly, B.E. Logan, The impact of new cathode
680 materials relative to baseline performance of microbial fuel cells all with the same
681 architecture and solution chemistry, Energy Environ. Sci.
682 DOI: 10.1039/C7EE00910K.
683 [38] State Environment Protection Administration, the Water and Wastewater
684 Monitoring Methods, fourth ed., China Environmental Science Press, Beijing,
685 2002.
686 [39] Y. Chen, J. Shen, L. Huang, Y. Pan, X. Quan, Enhanced Cd(II) removal with
687 simultaneous hydrogen production in biocathode microbial electrolysis cells in the
688 presence of acetate or $NaHCO_3$, Inter. J. Hydrogen Energy 41 (2016) 13368-13379.
689 [40] Z. He, F. Mansfeld, Exploring the use of electrochemical impedance
690 spectroscopy (EIS) in microbial fuel cell studies, Energy Environ. Sci. 2 (2009)
691 215-219.
692 [41] D. Wu, L. Huang, X. Quan, G. Li Puma, Electricity generation and bivalent
693 copper reduction as a function of operation time and cathode electrode material in
694 microbial fuel cells, J. Power Sources 307 (2016) 705-714.
695 [42] W. Li, G. Sheng, X. Liu, H. Yu, Recent advances in the separators for microbial
696 fuel cells, Bioresour. Technol. 102 (2011) 244-252.
697 [43] K.J. Chae, M.J. Choi, K.Y. Kim, F.F. Ajayi, W. Park, C.W. Kim, I.S. Kim,
698 Methanogenesis control by employing various environmental stress conditions in
699 two-chambered microbial fuel cells, Bioresour. Technol. 101 (2010) 5350-5357.
700 [44] T.H.J.A. Sleutels, R. Lodder, H.V.M. Hamelers, C.J.N. Buisman, Improved
701 performance of porous bio-anodes in microbial electrolysis cells by enhancing mass
702 and charge transport, Inter. J. Hydrogen Energy 34 (2009) 9655-9661.
703 [45] R.A. Rozendal, H.V.M. Hamelers, G.J.W. Euverink, S.J. Metz, C.J.N. Buisman,
704 Principle and perspectives of hydrogen production through biocatalyzed
705 electrolysis, Inter. J. Hydrogen Energy 31 (2006) 1632-1640.
706 [46] M.C. Dictor, C. Joulian, S. Touzé, I. Ignatiadis, D. Guyonnet, Electro-stimulated
707 biological production of hydrogen from municipal solid waste, Inter. J. Hydrogen
708 Energy 35 (2010) 10682-10692.

[47] P.A. Selembo, M.D. Merrill, B.E. Logan, The use of stainless steel and nickel alloys as low-cost cathodes in microbial electrolysis cells, J. Power Sources 190 (2009) 271-278.
[48] Y. Ruiz, J.A. Baeza, A. Guisasola, Enhanced performance of bioelectrochemical hydrogen production using a pH control strategy, ChemSusChem 8 (2015) 389-397.
[49] X. Liu, W. Li, H. Yu, Cathodic catalysts in bioelectrochemical systems for energy recovery from wastewater, Chem. Soc. Rev. 43 (2014) 7718-7745.
[50] H. Cesiulis, A. Baltutiene, M. Donten, M.L. Donten, Z. Stojek, Increase in rate of electrodeposition and in Ni(II) concentration in the bath as a way to control grain size of amorphous/nanocrystalline Ni-W alloys, J. Solid State Electrochem. 6 (2002) 237-244.
[51] J.C. Tokash, B.E. Logan, Electrochemical evaluation of molybdenum disulfide as a catalyst for hydrogen evolution in microbial electrolysis cells, Inter. J. Hydrogen Energy 36 (2011) 9439-9445.
[52] Y. Shen, H. Xu, P. Xu, X. Wu, Y. Dong, L. Lu, Electrochemical catalytic activity of tungsten trioxide-modified graphite felt toward VO_2^+/VO^{2+} redox reaction, Electrochim. Acta 132 (2014) 37-41.
[53] E. Yavuz, K.V. Özdokur, İ. Çakar, S. Koçak, F.N. Ertaş, Electrochemical preparation, characterization of molybdenum-oxide/platinum binary catalysts and its application to oxygen reduction reaction in weakly acidic medium, Electrochim. Acta 151 (2015) 72-80.
[54] J.L. Varanasi, A.K. Nayak, Y. Sohn, D. Pradhan, D. Das, Improvement of power generation of microbial fuel cell by integrating tungsten oxide electrocatalyst with pure or mixed culture biocatalysts, Electrochim. Acta 199 (2016) 154-163.
[55] C. He, Z. Mu, H. Yang, Y. Wang, Y. Mu, H. Yu, Electron acceptors for energy generation in microbial fuel cells fed with wastewaters: A mini-review, Chemosphere 140 (2015) 12-17.
[56] Q. Wang, L. Huang, Y. Pan, X. Quan, G. Li Puma, Impact of Fe(III) as an effective electron-shuttle mediator for enhanced Cr(VI) reduction in microbial fuel cells: Reduction of diffusional resistances and cathode overpotentials, J. Hazard. Mater. 321 (2016) 896-906.
[57] W. Li, H. Yu, Z. He, Towards sustainable wastewater treatment by using microbial fuel cells-centered technologies, Energy Environ. Sci. 7 (2014) 911-924.
[58] R.O. Ramabhadran, J.E. Mann, S.E. Waller, D.W. Rothgeb, C.C. Jarrold, K. Raghavachari, New insights on photocatalytic H_2 liberation from water using transition-metal oxides: Lessons from cluster models of molybdenum and tungsten oxides, J. Am. Chem. Soc. 135 (2013) 17039-17051.

Table 1 Separation factor, product yield, and operational efficiencies in various stacked BESs.

Fig. 1 Types of stacked BESs in this study

Fig. 2 W (A) and Mo (B) deposition, cathode potentials (C) and circuital current (D)

in the stacked BES-3-1. Applied voltage (E) and hydrogen production (F) in the 1# unit of the BES-3-1.

Fig. 3 Voltage output and power density (A, C and E), and anode and cathode potentials (B, D and F) in the stacked BES-3-1, and controls of the single 1# or 2# units with the components of W(VI) and Mo(VI) (A and B), individual Mo(VI) (C and D), and single W(VI) (E and F).

Fig. 4 Naked eye (A, B, C and D) and SEM (E, F, G and H) observation, EDS analysis (I, J, K and L) and XED determination (M, N, O and P) on the cathodes of the 1# (A, E, I, M, C, G, K and O) and 2# units (B, F, J, N, D, H, L and P) before (A, E, I, M, B, F, J and N) and after (C, G, K, O, D, H, L and P) exposed to air for 24 h (2 cycle operation).

Fig. 5 XPS analysis for W (A, C, E and G) and Mo (B, D, F and H) elements on the cathodes of the 1# (A, B, E, and F) and 2# units (C, D, G and H) before (A, B, C and D) and after (E, F, G and H) exposed to air for 24 h.

Fig. 6 W (A) and (B) Mo deposition in the different units of the stacked BESs and the associated cathode potential (C) and circuital current (D).

Fig. 7 W (A) and Mo (B) deposition, separation factor (C), cathode potential (D), and circuital current (E) in the 1# and 2# units of BES-3-1, as well as applied voltage as a function of the operational cycle.

Table 1

Table 1 Separation factor, product yield, and operational efficiencies in various stacked BESs.

Stacked BESs			BES-1-1	BES-2-1	BES-3-1	BES-2-2	BES-3-3	BES-4-1	BES-1-1-1	BES-3-2-1	BES-2-2-2
Separation factor	1#		6.3 ± 1.1	8.8 ± 0.2	8.1 ± 0.2	4.7 ± 0.7	4.1 ± 1.1	8.1 ± 0.6	7.5 ± 1.2	4.2 ± 0.7	3.3 ± 0.7
	2#		5.7 ± 0.8	6.4 ± 0.6	7.9 ± 0.5	4.7 ± 1.2	3.8 ± 0.9	4.3 ± 0.1	6.5 ± 0.9	3.9 ± 1.1	3.8 ± 0.9
	3#		---	---	---	---	---	---	6.9 ± 1.1	3.7 ± 0.9	3.5 ± 0.8
Hydrogen production (m^3/m^3 d)	1#		0.00 ± 0.00	0.00 ± 0.00	0.34 ± 0.10	0.00 ± 0.00	0.00 ± 0.00	0.83 ± 0.20	0.00 ± 0.00	0.82 ± 0.10	0.00 ± 0.00
	2#		0.00 ± 0.00	0.00 ± 0.00	0.00 ± 0.00	0.00 ± 0.00	0.00 ± 0.00	0.00 ± 0.00	0.00 ± 0.00	0.33 ± 0.20	0.00 ± 0.00
	3#		---	---	---	---	---	---	0.00 ± 0.00	0.00 ± 0.00	0.00 ± 0.00
Product yield (mol/mol COD)	1#	W	0.08 ± 0.02	0.11 ± 0.03	0.09 ± 0.01	0.13 ± 0.01	0.14 ± 0.02	0.08 ± 0.01	0.12 ± 0.02	0.13 ± 0.01	0.08 ± 0.02
		Mo	0.23 ± 0.03	0.25 ± 0.04	0.26 ± 0.02	0.21 ± 0.03	0.20 ± 0.01	0.26 ± 0.02	0.25 ± 0.01	0.26 ± 0.02	0.25 ± 0.01
		H_2	0.00 ± 0.00	0.00 ± 0.00	0.87 ± 0.03	0.00 ± 0.00	0.00 ± 0.00	0.56 ± 0.01	0.00 ± 0.00	0.65 ± 0.02	0.00 ± 0.00
	2#	W	0.09 ± 0.01	0.11 ± 0.02	0.08 ± 0.01	0.12 ± 0.02	0.11 ± 0.01	0.07 ± 0.01	0.09 ± 0.01	0.10 ± 0.02	0.11 ± 0.02
		Mo	0.24 ± 0.01	0.26 ± 0.02	0.23 ± 0.01	0.25 ± 0.02	0.23 ± 0.01	0.20 ± 0.01	0.26 ± 0.02	0.25 ± 0.02	0.23 ± 0.01
		H_2	0.00 ± 0.00	0.00 ± 0.00	0.00 ± 0.00	0.00 ± 0.00	0.00 ± 0.00	0.00 ± 0.00	0.00 ± 0.00	0.49 ± 0.02	0.00 ± 0.00
	3#	W	---	---	---	---	---	---	0.11 ± 0.01	0.07 ± 0.01	0.10 ± 0.02
		Mo	---	---	---	---	---	---	0.19 ± 0.02	0.21 ± 0.01	0.23 ± 0.00
		H_2	---	---	---	---	---	---	0.00 ± 0.00	0.00 ± 0.00	0.00 ± 0.00
CE_{an} (%)	1#		55 ± 3	56 ± 4	52 ± 1	43 ± 2	39 ± 2	49 ± 5	50 ± 3	49 ± 7	43 ± 3
	2#		47 ± 2	39 ± 4	42 ± 3	45 ± 5	44 ± 3	38 ± 3	49 ± 6	51 ± 2	45 ± 5
	3#		---	---	---	---	---	---	39 ± 2	47 ± 1	48 ± 7
CE_{ca} (%)	1#		75 ± 2	73 ± 7	70 ± 5	83 ± 5	65 ± 6	67 ± 8	76 ± 7	77 ± 1	64 ± 6
	2#		65 ± 7	81 ± 6	67 ± 1	78 ± 5	71 ± 7	83 ± 4	82 ± 3	69 ± 5	68 ± 5
	3#		---	---	---	---	---	---	81 ± 7	79 ± 4	82 ± 3
η_{sys} (%)			19 ± 1	23 ± 4	21 ± 0	17 ± 1	25 ± 1	15 ± 0	19 ± 1	22 ± 1	23 ± 2

Figure 1

Click here to download high resolution image

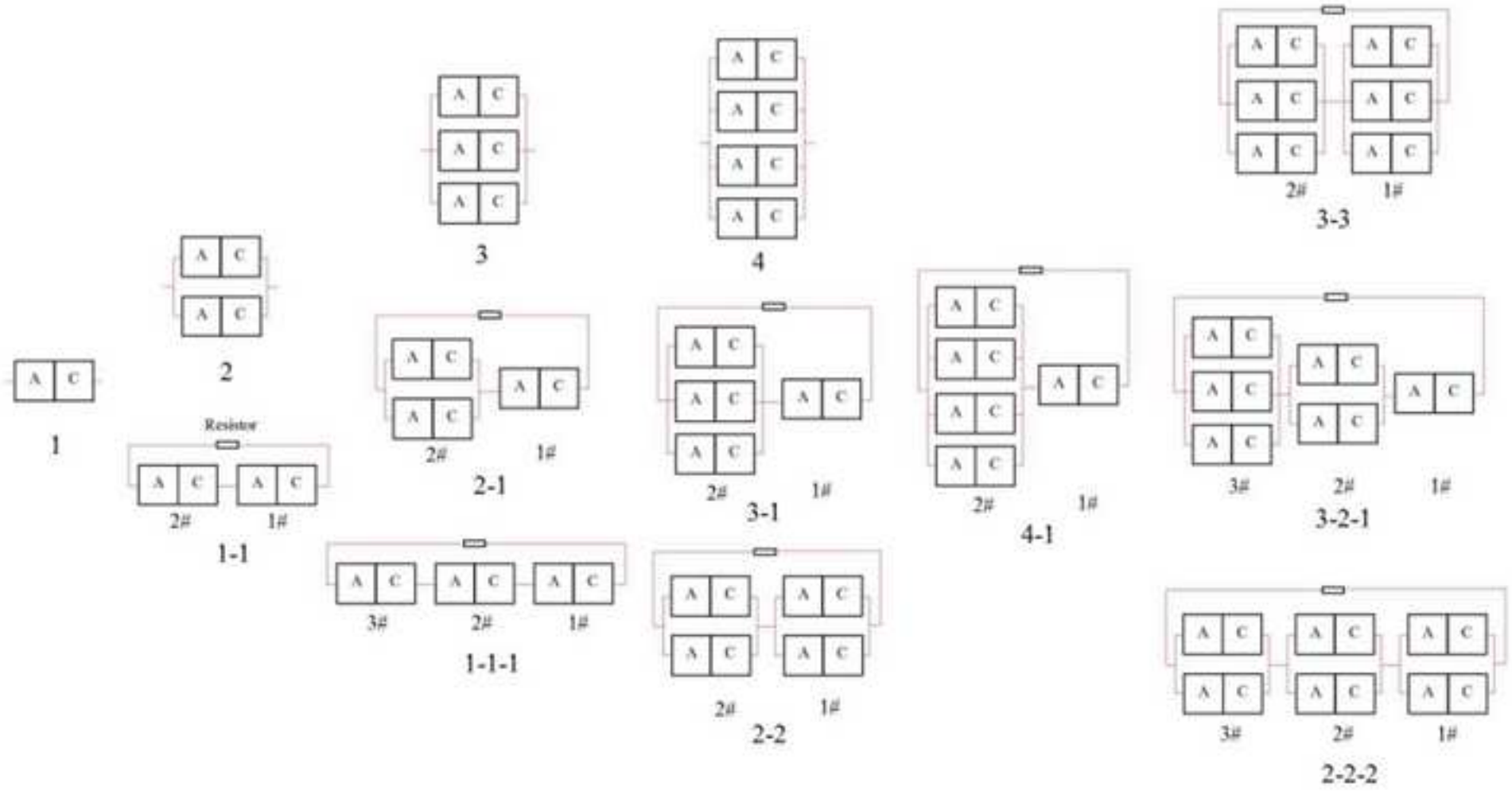

Figure 2

Click here to download high resolution image

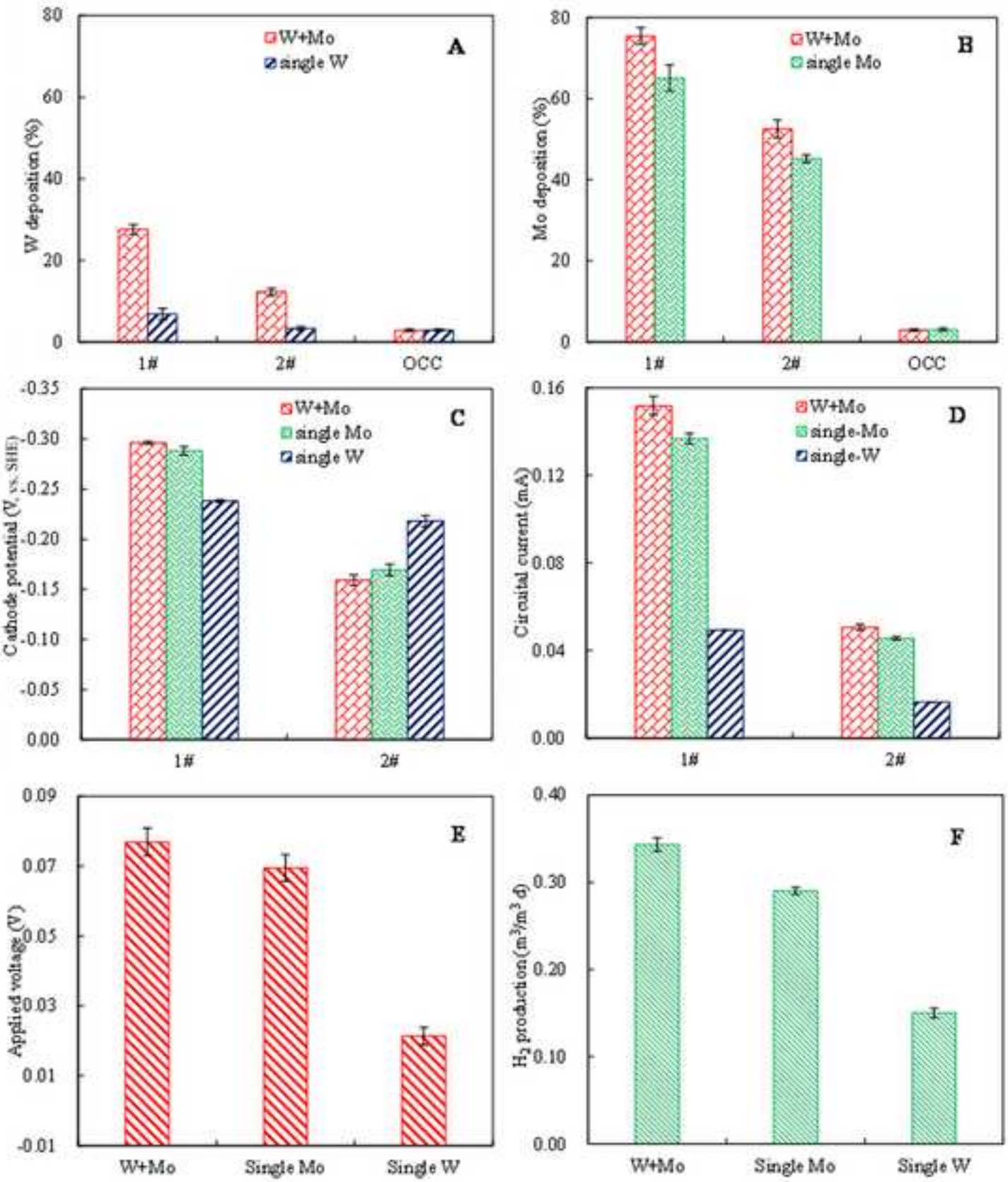

Figure 3

Click here to download high resolution image

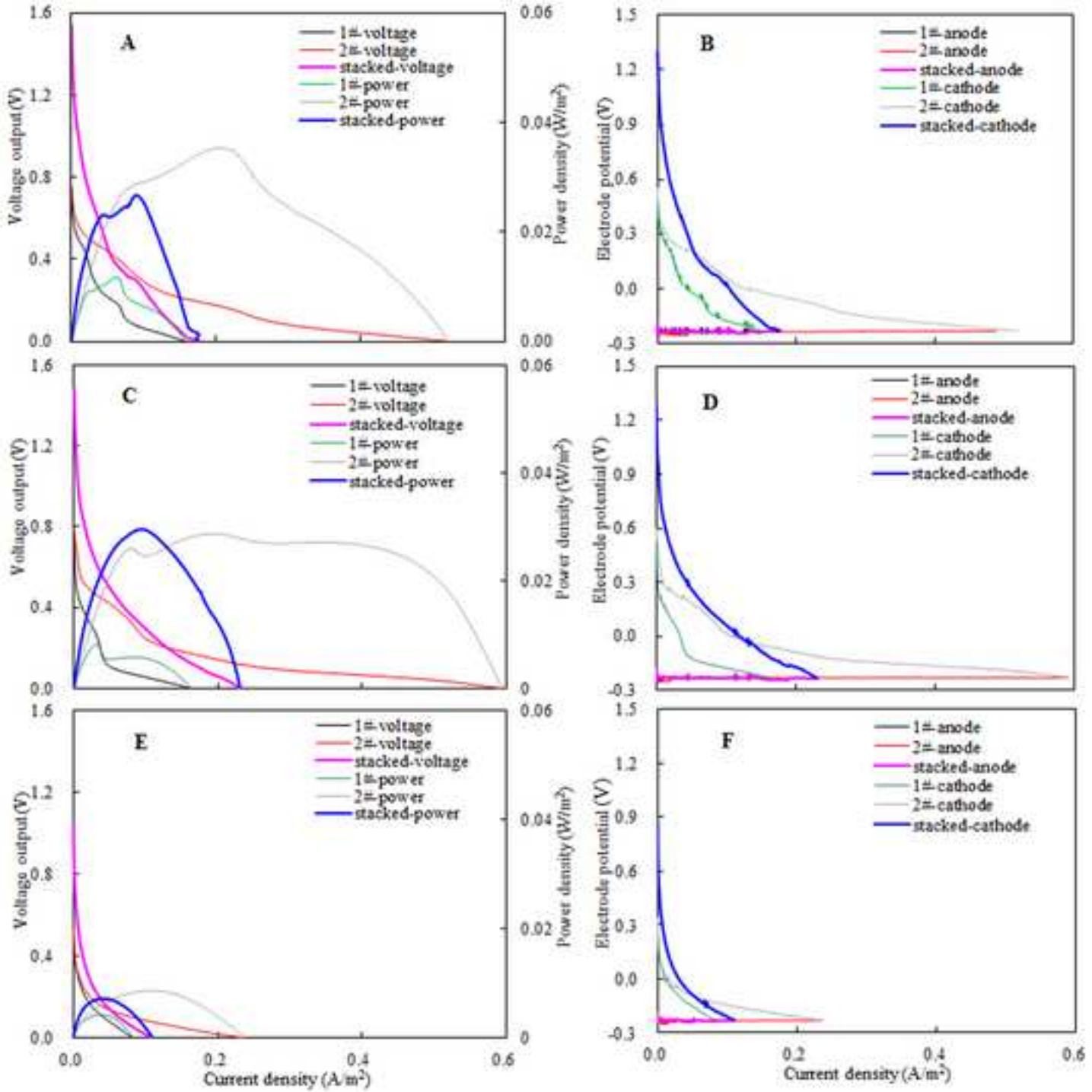

Figure 4

Click here to download high resolution image

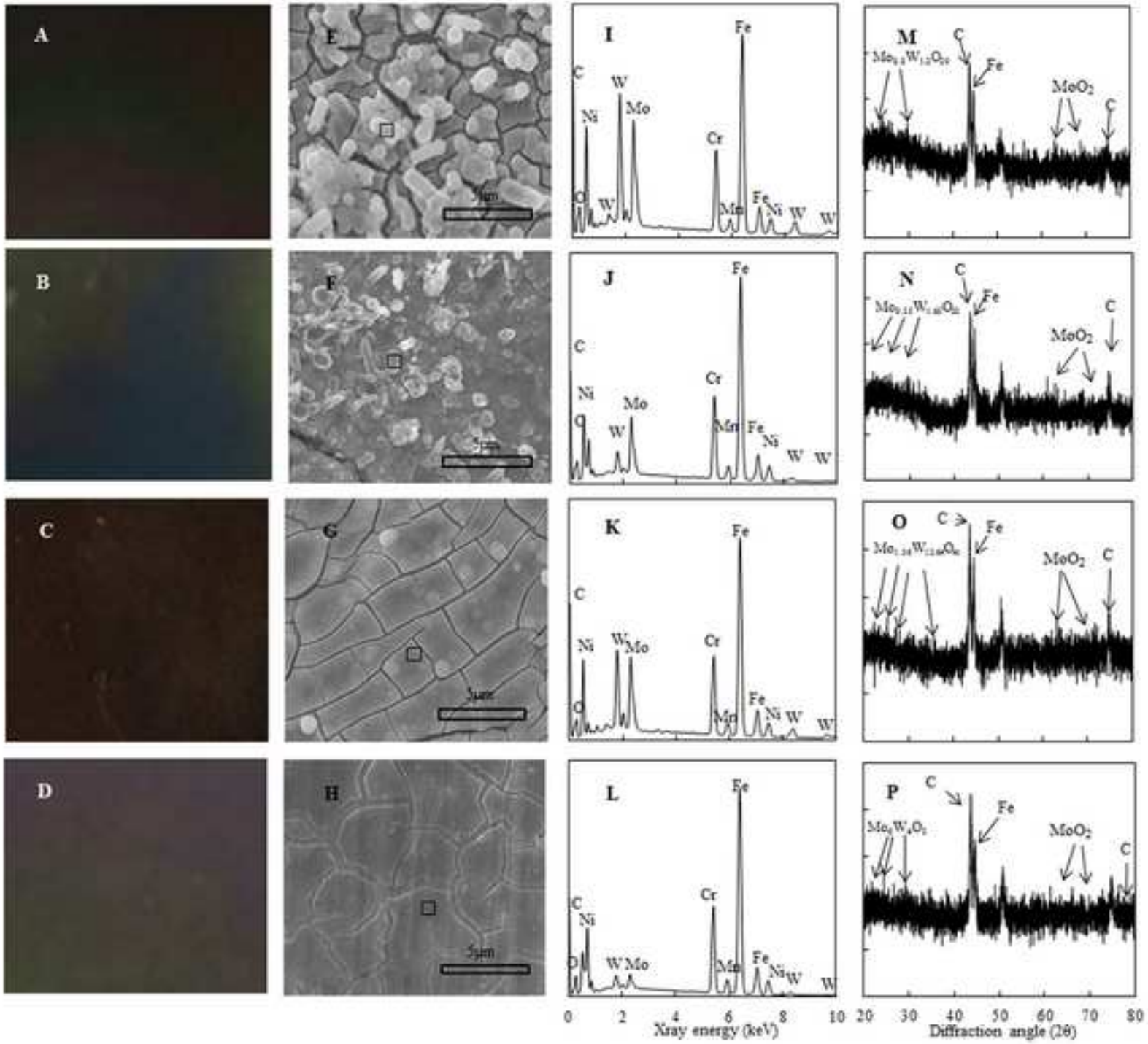

Figure 5

Click here to download high resolution image

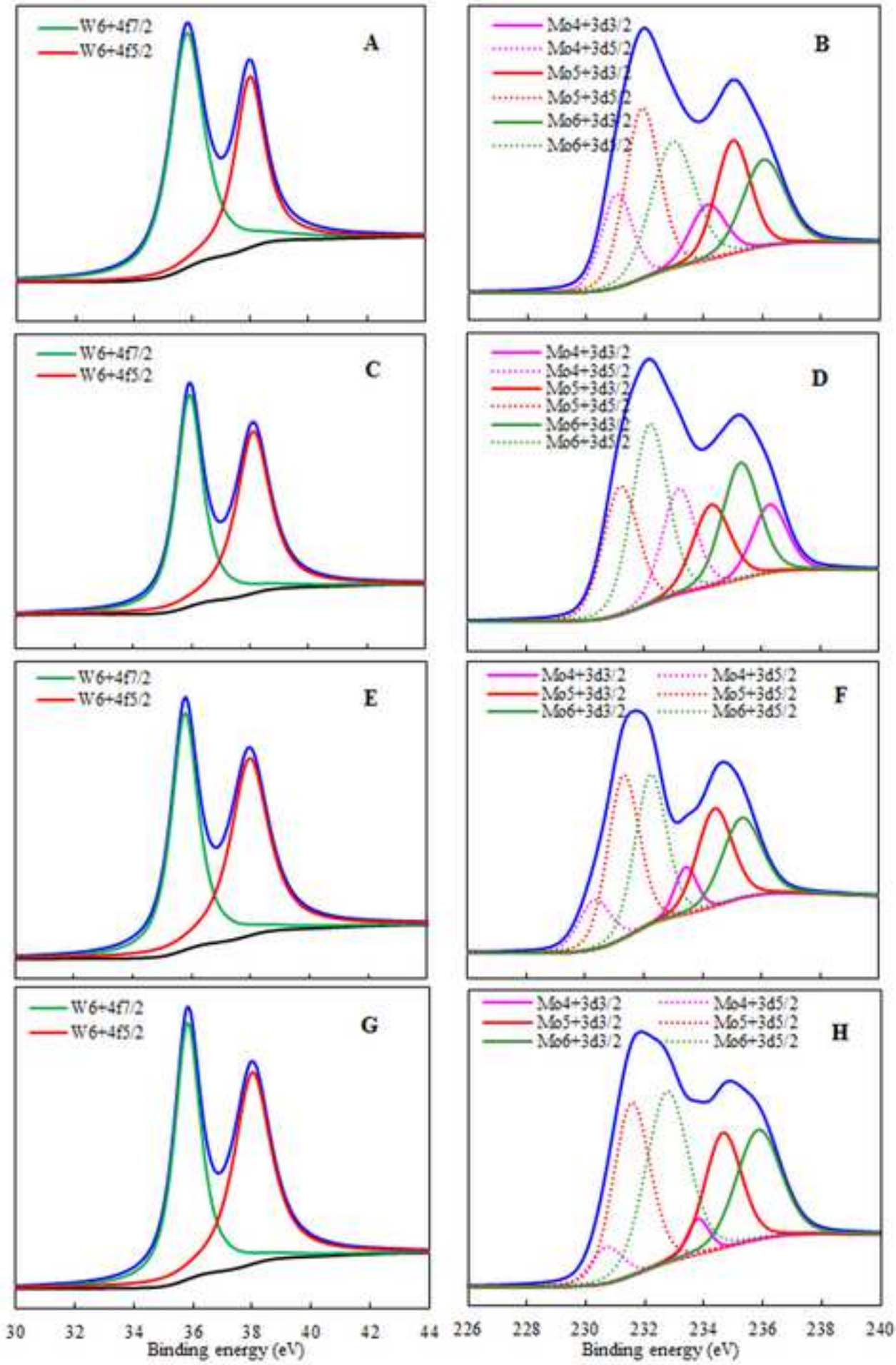

Figure 6

Click here to download high resolution image

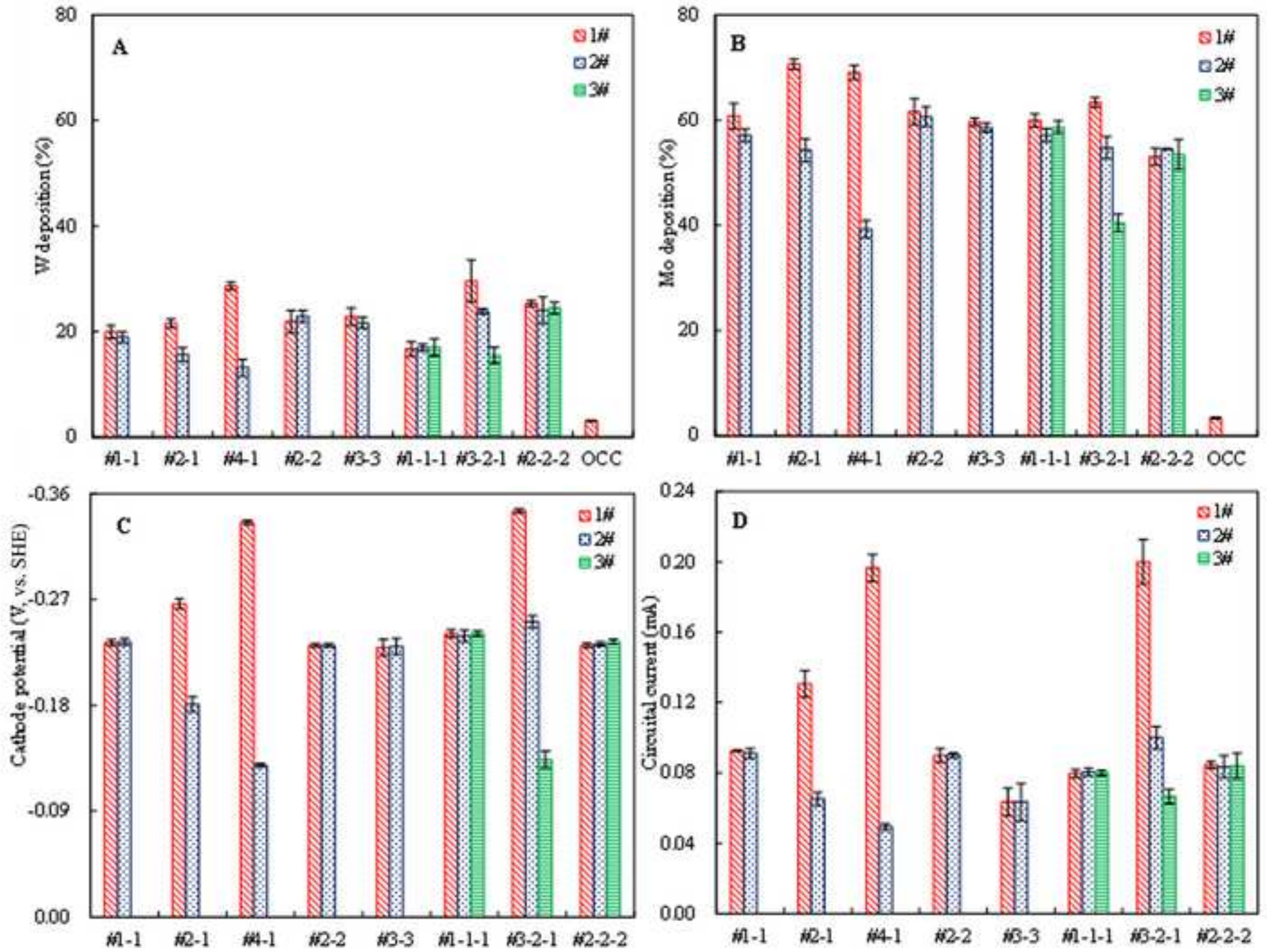

Figure 7

Click here to download high resolution image

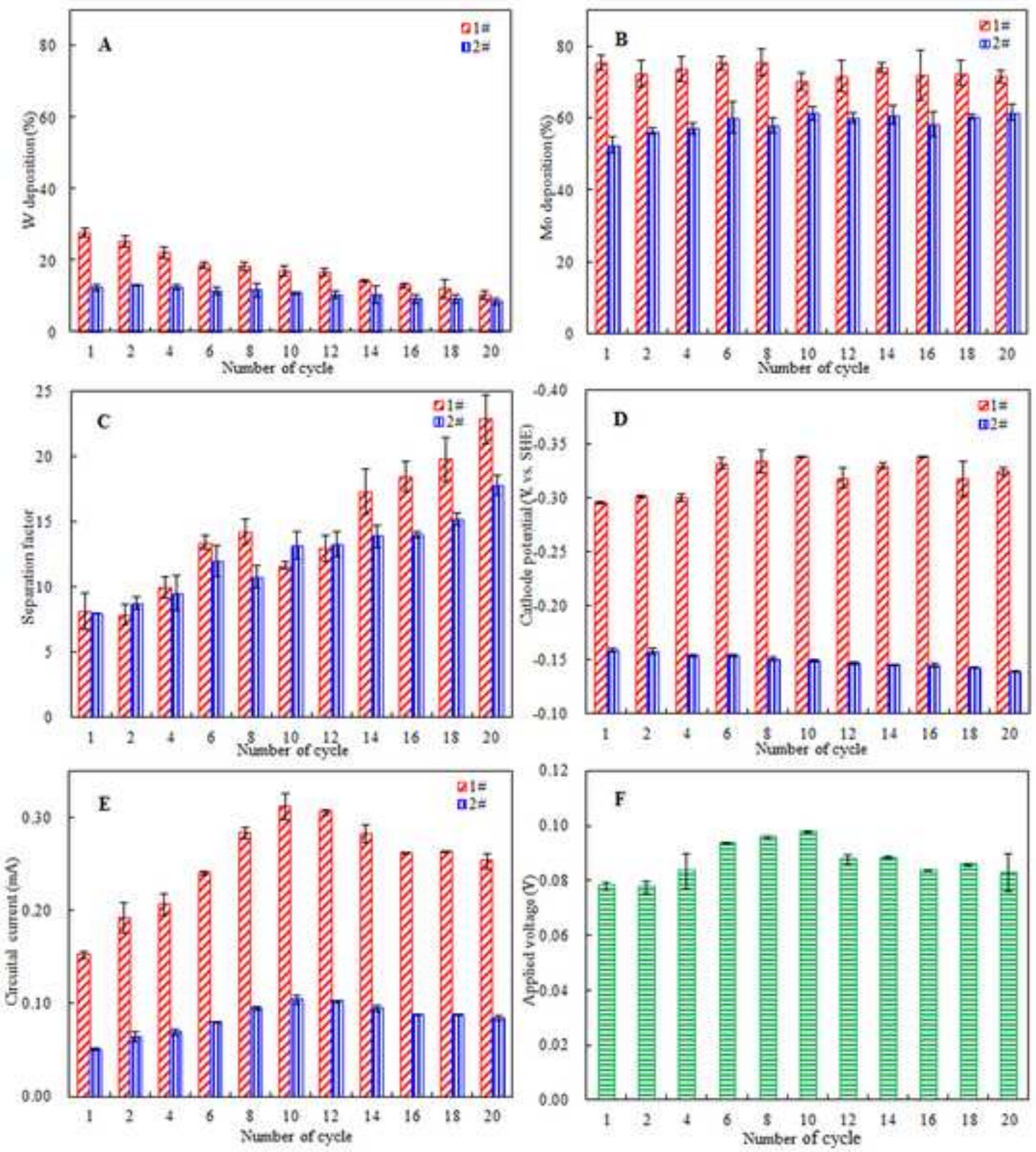

Supplementary Material

Click here to download Supplementary Material: Supporting Material.doc